Real-Time Investigation of Ultrafast Dynamics through Time-Stretched Dispersive Fourier Transform in Mode-Locked Fiber Lasers

Kuen Yao Lau, Yudong Cui, Xiaofeng Liu,* and Jianrong Qiu*

Real-time investigation in mode-locked fiber lasers (MLFLs) is important to understand the ultrafast dynamics before, during, and after the formation of stable laser pulses. However, the experimental measurement of these dynamics is restricted by the resolution of conventional oscilloscopes. The development of a time-stretched dispersive Fourier transform (TS-DFT) technique provides the shot-to-shot measurement of mapping the spectral information of an ultrashort optical pulse into time-stretched waveform in the MLFL. Here, the recent progress and development of various fascinating dynamics in the MLFL, including the study of birth, evolution, and extinction process in MLFL, different types of MLFL, and complex motion dynamics in MLFL, have been reviewed. The issues and challenges encountered in this research area are discussed and several recommendations are suggested to overcome these problems. The integration of the TS-DFT technique is expected to provide deeper insight into the real-time investigation of various dynamics in the MLFL by displaying fascinating phenomenon and revealing unexplored trajectories.

1. Introduction

A mode-locked fiber laser (MLFL) generates ultrashort and intense flashes of light, constituting a major advance in the development of ultrafast fiber optics. The MLFL contributes to not only industrial fields by offering huge economic benefits because of its extensive applications in optical frequency metrology,[1]

K. Y. Lau
Institute of Light+X Science and Technology, Faculty of Electrical Engineering and Computer Science
Ningbo University
Ningbo 315211, China
Y. Cui, J. Qiu
College of Optical Science and Engineering and State Key Lab of Modern Optical Instrumentation
Zhejiang University
Hangzhou 310027, China
E-mail: qjr@zju.edu.cn
X. Liu
School of Materials Science and Engineering
Zhejiang University
Hangzhou 310027, China
E-mail: xfliu@zju.edu.cn

astronomical observation,[2] and material processing,[3] but also facilitates scientific research by providing an excellent platform to investigate its diversified dynamics through real-time measurement. Mode-locking is an effective technique to generate picosecond to femtosecond laser pulses, whilst most longitudinal modes of the laser cavity are phase-locked and constructively interfere with each other to form ultrashort and intense laser pulses.[4,5] However, this nearly perfect periodicity only occurs in stable mode-locking operation. Prior to stable operation, the initiation stage always starts from noise fluctuation and experiences several evolution stages, which are highly unique and nonrepetitive.[6] The initial signal always starts with a random noise background, such as an amplified spontaneous emission, followed by a raised relaxation oscillation, which experiences a sequence of stages until a stable mode-locking stage was achieved. The duration of this process from the first laser spike to stable mode-locking is defined as the nascent time of the laser. Some transient features at the nascent stage of this laser can be expressed by the rate equations[7]

$$\frac{du}{dt} = R_p - uB_s q - \frac{u}{T_u} \tag{1}$$

$$\frac{dq}{dt} = uB_s q - \frac{q}{l} + \frac{u}{p_m T_u} \tag{2}$$

where u and q denote the population inversion and photon number in the laser cavity, respectively. R_p is the pumping rate, B_s is the Einstein coefficient given by $B_s = 1/(p_m T_u)$, where p_m is the number of cavity modes coupled to the fluorescent line, which is given by $p_m = 8\pi\nu^2 \Delta\nu V/c^3$, where ν is the carrier frequency of photons, $\Delta\nu$ is the bandwidth of the laser medium, V is the mode volume within the laser cavity, and c is the speed of light in vacuum. T_u is the lifetime of the upper-laser level, and l is the photon lifetime related to cavity loss. In the past decades, the experimental investigation of buildup and evolution dynamics in the MLFL from initial noise signal to stable mode-locking stage has been a difficult task due to speed limitations, i.e., low response bandwidth and slow scan rate of the oscilloscopes. For instance, oscilloscopes working on scanned Fabry–Pérot interferometers could

not operate with a speed faster than a few kHz,[8] whereas the detector arrays employed in other types of oscilloscopes could not exceed 20 kHz.[9] Therefore, the integration of a technique to resolve the real-time shot-to-shot information for the buildup and evolution dynamics in the MLFL has been luring great attention among the scientific community in recent years.

In the MLFL, a soliton or solitary wave is a wave packet exhibiting self-reinforcing which keep its original shape after wave propagates at a constant velocity.[10] This is due to the interaction of both nonlinearity and dispersive effects, which produce localized waveforms and cancel out each other after the wave propagation.[11] The presence of the nonlinear Kerr effect contributes to the direct influence of light intensities on the refractive index of a material. Subsequently, the Kerr effect cancels the dispersion effect when the pulse exhibits the right shape. This leads to a constant pulse shape over time, which is called the soliton. Therefore, stable optical solitons can be formed and propagated in an optical fiber, which have been extensively applied in optical communications,[12,13] mathematical physics,[14] optical transmission lines, and fiber lasers.[15] Besides these applications, various interesting dynamics were observed during the generation of stable mode-locked pulses, which is very important to understand the underlying physics and mechanism of nonlinear ultrafast laser optics.

However, the dynamics of MLFL are difficult to be measured through conventional instruments, i.e., the optical spectrum analyzer or the oscilloscope. Therefore, the exploration of a new technique to investigate the MLFL dynamics is important to solve the challenges encountered by these conventional approaches. The development of time-stretched dispersive Fourier transform (TS-DFT) technology provides an experimental real-time measurement to directly observe the MLFL dynamics by stretching an incident ultrashort laser pulse through a long dispersive medium with large group velocity dispersion (GVD).[16] The large GVD is capable of mapping the spectral information of an ultrashort optical pulse into time-stretched waveform. The shot-to-shot measurement offers the observation of both buildup and internal dynamics in versatile soliton, such as soliton,[7] soliton molecules,[16] soliton trapping,[17] soliton breathing,[18] soliton collision,[19] soliton rains,[20] and multisoliton complexes.[21] Based on real-time recorded data, shot-to-shot spectral interferograms display a variety of motion dynamics and relative phase evolution, constituting the intramolecular energy flow facilitated by gain dynamics and soliton interactions.[21]

Here, we review the birth, evolution, and extinction dynamics of solitons observed at different intracavity GVD in MLFL, i.e., soliton, dissipative soliton, stretched pulse, and soliton similariton through the TS-DFT technique. Next, we review the dynamics of different types of MLFL, i.e., high repetition rate achieved through harmonic mode-locking regime and counterpropagating solitons through bidirectional MLFL cavity. Moreover, the complex motion dynamics in MLFL, i.e., soliton molecules, soliton breathing, soliton bifurcation, soliton explosion, soliton trapping, and optical rogue wave were comprehensively discussed. More information about the underlying physics of the TS-DFT technique and its applications in MLFL dynamics[22,23] and other fields of optical physics[24–27] was previously reviewed. In comparison to the reviews of Wang et al. and Huang et al.[22,23] which were officially available on January 2020 and June 2020, respec-

tively, we provide a more recent review of the progress and development in the diversified dynamics of the MLFL probed by using the TS-DFT technique.

2. Underlying Physics for TS-DFT Technique

The pulse train of an MLFL was measured with an oscilloscope through a photodetector. However, a conventional oscilloscope consisting of a grating and line sensor exhibits a readout speed, which is several orders slower than the build-up and evolution dynamics in an MLFL.[28] Owing to the speed limitation, the MLFL pulses with durations shorter than 10 ps could hardly be resolved even by employing a high-speed oscilloscope with a larger bandwidth than conventional ones. Therefore, an additional technique should be applied to resolve the build-up and evolution process in the MLFL. The speed limitation of a conventional oscilloscope was solved by the TS-DFT technique, which enables continuous shot-to-shot measurements in real-time. The fast response time of the photodetection in the TS-DFT system contributes to the feasibility of resolving the shot-to-shot spectral information over consecutive roundtrips at a scan rate which is measurable by a high-speed oscilloscope. The TS-DFT technique provides the linear dispersion of localized MLFL pulses in a dispersive medium, mapping the spectral information of an ultrashort optical pulse into time-stretched waveform with large GVD. Therefore, the pulse width was stretched from fs and ps scale to sub-ns or ns scale, effectively mitigating the bandwidth requirement of high-speed sampling instrument, without any loss of the spectral information.[25] Nevertheless, the real-time measurement of the TS-DFT technique is typically feasible for pulses with durations shorter than 10 ps and unviable for a continuous wave (CW) or pulsed lasers with longer duration. The group delay dispersion of the TS-DFT determines its spectral resolution ($\Delta\lambda_{\text{res}}$), which is approximately given by[29,30]

$$\Delta\lambda_{\text{res}} = \frac{\lambda_0}{\sqrt{\frac{|D|Lc}{2}}} \tag{3}$$

where λ_0 is the center wavelength of an MLFL, D is the dispersion parameter, L is the length of the dispersive medium, and c is the speed of light in vacuum. The limitation of TS-DFT technique with respect to pulse propagation in a dispersive medium could be deduced from partial differential equation

$$i\frac{\partial A}{\partial z} = \frac{\beta_2}{2}\frac{\partial^2 A}{\partial t^2} \tag{4}$$

where $A(z,t)$ is the field amplitude envelope and β_2 is the dispersion coefficient given as

$$\beta_2 = \frac{-D(\lambda_0)^2}{2\pi c} \tag{5}$$

The schematic diagram of the TS-DFT principle is depicted in **Figure 1**.[22] The pulse width of an incident ultrashort laser pulse was gradually stretched over a long dispersive medium and eventually, the pulse waveform exhibits a close envelope to the
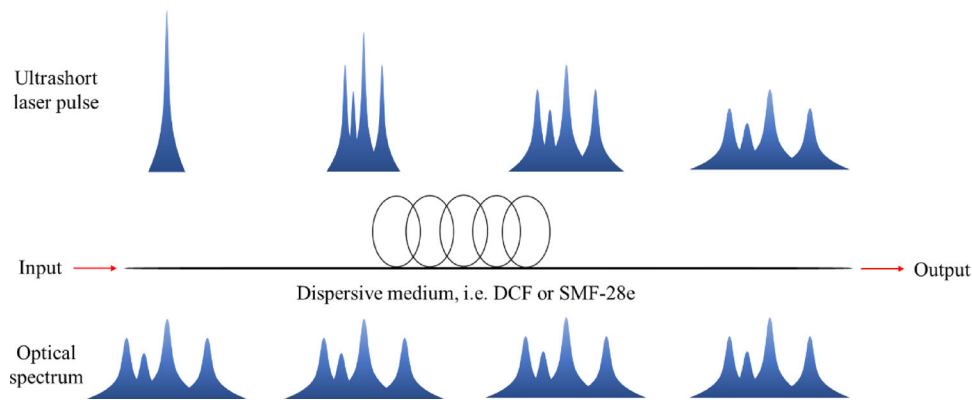
**ADVANCED
SCIENCE NEWS**

www.advancedsciencenews.com

**LASER
& PHOTONICS
REVIEWS**

www.lpr-journal.org

Figure 1. Schematic diagram for the underlying physics of the TS-DFT technique. Reproduced with permission.[22] Copyright 2020, IOP Publishing Ltd.

optical spectrum at the output. The mapping relationship can be expressed as[31,32]

$$\Delta\tau = \Delta\lambda \cdot |D| \cdot L \qquad (6)$$

where $\Delta\tau$ is the duration of stretched pulses typically about a few to tens of nanosecond, $\Delta\lambda$ is the spectral width of incident pulses, and D and L are the dispersion parameter and length of the dispersive medium, respectively. The mapping relationship reveals the independence of the TS-DFT technique on whether the dispersive medium has positive or negative GVD, but this condition is only valid for ultrashort pulses with no or small chirping features. A wideband ultrashort pulse could be stretched more efficiently through the TS-DFT technique than a narrowband ultrashort pulse.[33] The mapping of the spectrogram with the TS-DFT technique could be validated with optical spectrum measurement, whereas the overlapping of the optical spectrum to the time-stretched waveform generates almost the same spectral intensity envelope. The practical conditions to employ the TS-DFT include propagating the pulse in linear regime and reaching pulse propagation in the far field dispersion regime with a dispersive medium. The ultrashort laser pulse is designed to provide ultrafast transient events, which was stretched in time domain by a dispersive medium, such as a dispersion compensating fiber (DCF) or a single-mode fiber (SMF-28e), detected by a photodetector and monitored by a high-speed oscilloscope. The subsequent stretched pulse should be avoided from overlapping. The recorded temporal waveform data of the stretched pulses are segmented into several pieces with each segment length equal to the pulse period. These data pieces were rearranged as a function of round-trip number (RTN) to construct a pulse evolution image. By matching the stretched pulse waveform and average optical spectrum, the time coordinate can be converted to a wavelength coordinate, thus the pulse evolution image was converted to real-time spectra. As a result, the ultrafast transient phenomenon can be observed from these real-time spectra.

In the TS-DFT system, a long DCF or SMF-28e is commonly utilized as the dispersive medium, which provides large normal and anomalous GVD, respectively, to map the broadband spectrum of an ultrashort optical pulse into a time-stretched waveform. Besides the DCF and SMF-28e, various dispersive media, i.e., chirped fiber Bragg gratings, large spatial chirp, and chromo-

modal dispersion were employed for the TS-DFT system at different wavebands.[34–36] In the C-band, SMF-28e and DCF are still the most popular choice for the TS-DFT system due to their simplicity, easy availability, and cost-effectiveness. To avoid spectral distortion and ensure effective mapping, the peak power should be maintained at a reasonable range.[37] According to energy conservation law, the peak power will be reduced after the TS-DFT system, leading to degradation of the signal-to-noise ratio. A high peak power of an incident pulse causes excessive accumulation of nonlinear phase shift, leading to the distortion of the pulse waveform stretched by the TS-DFT technique. On the other hand, the weak peak power of the incident pulse leads to the submersion of pulse signals by background noises. Nevertheless, the weak peak power can always be amplified by several optical amplifiers, i.e., stimulated Raman scattering distributed optical amplifier, semiconductor optical amplifier, and rare-earth-doped fiber amplifier.

Apart from peak power, the parameters of incident pulses and dispersive medium determine the basic properties of recorded data by the TS-DFT system. The frame rate of TS-DFT is equal to the pulse repetition rate, which is typically several to tens of MHz and is much larger than that of a conventional optical spectrum analyzer.[22] Moreover, there are several issues with the TS-DFT technique. For instance, the pulse waveforms stretched through the TS-DFT system should not be overlapped.[38] Therefore, it is difficult to analyze an ultrashort pulse with an extremely high repetition rate. Besides that, the spectral resolution of the TS-DFT technique is influenced by the sampling rate of the real-time oscilloscope, the bandwidth of the photodetector, the second-order dispersion coefficient, the length of dispersive medium and the repetition rate of the ultrashort optical pulses.[22] These parameters should be carefully considered before the real-time experimental measurement was performed.

3. Real-Time Investigation of MLFL Dynamics

The real-time investigation of the fascinating dynamics in the MLFL was conducted through the TS-DFT technique. These investigations were done in terms of the study of birth, evolution, and extinction process in MLFL, several techniques of MLFL cavities, and complex motion dynamics in MLFL. For the study of birth, evolution and extinction process in the MLFL, the intracavity GVDs were designed with anomalous, normal,

dispersion-managed (DM), and near-zero in normal regimes for soliton, dissipative soliton, stretched pulse, and soliton similariton, respectively. An MLFL relies on the laser cavity design to achieve desired ultrafast laser performances, i.e., high repetition rate using harmonic mode-locking and counterpropagating solitons using bidirectional MLFL setup. Some complex motion dynamics in the MLFL, i.e., soliton molecules, soliton breathing, soliton bifurcation, soliton explosion, soliton trapping, and optical rogue wave were comprehensively investigated.

3.1. Birth, Evolution, and Extinction Dynamics in MLFL

The MLFL can operate in four GVD regimes, i.e., anomalous, normal, DM, and near-zero in normal regimes, for soliton, dissipative soliton, stretched pulse, and soliton similariton, respectively. Hereinafter, the real-time investigation of the buildup, evolution and extinction dynamics was discussed for these four MLFL pulses working at different intracavity GVD regimes.

3.1.1. Soliton

The soliton is robust over long-distance propagation. The investigation of the real-time buildup and evolution process is important to understand its formation and extinction mechanisms.[39] The energy redistribution during the formation of the soliton among various interval modes becomes complex before the generation of stationary soliton. For instance, the buildup and evolution process of the soliton dynamics was studied in a mode-locked erbium-doped fiber laser (EDFL) integrated with a hybrid saturable absorber consisting of carbon-nanotube saturable absorber (CNT-SA) and nonlinear polarization rotation (NPR) method.[7] The CNT-SA is important to suppress the environmental perturbations caused by the temperature, mechanical and pumping strength variations. Therefore, fewer unstable Q-switched lasing, i.e., five lines prior to the formation of the stable soliton-MLFL (S-MLFL) was observed. Instead, the integration of only the NPR technique shows larger number of unstable Q-switched lasers with 76 and 189 lines under weak and strong fluctuation of pumping strength, respectively. The S-MLFL was generated through two processes. The first process consists of the raised relaxation oscillation (RO) stage, quasi-mode-locking (QML) stage, spectral beating stage, and finally stable mode-locking stage. The second process comprises an additional transient bound-state, prior to the final stable mode-locking stage. The real-time investigation of these dynamics was executed with a TS-DFT system comprising a 5 km long DCF with a dispersion of ≈-160 ps (nm km)$^{-1}$ that produces the delay of real-time spectral data by ≈24.5 µs. **Figure 2**a presents the buildup and evolution process of a stable S-MLFL in the first process. Five laser spikes with intervals of ≈80 µs were observed before the formation of a stable mode-locked laser. The spectral information of a stable mode-locked laser reveals the pulse-to-pulse interval of ≈38.03 ns as shown in Figure 2b. The characteristics of the S-MLFL were denoted by Kelly's sidebands from the spectral information.[40] As shown in Figure 2c, Q-switched mode-locking (Q-ML) and beating dynamics were observed in the fifth laser spike where the transition state occurs. The expanded views of the Q-ML are presented in Figure 2d,e. Multiple

subordinate pulses were presented in Figure 2e, where a dominant pulse exhibits the highest intensity among the multiple subordinate pulses in the laser cavity. The pulse-to-pulse interval of ≈38.03 ns matches with Figure 2b, which corresponds to the roundtrip time of the laser cavity. Furthermore, another real-time observation of the dynamics experiencing the initial noise background and quasi-continuous wave (QCW) to stable mode-locking stage was demonstrated in an S-MLFL integrated with CNT-SA.[41] The pulse intensity is continuously increased in the QCW stage. Then, the QCW laser pulse with a high-pulse intensity experiences a decreasing trend and finally forms the stable mode-locking stage. Figure 2f reveals the complex formation process for stationary single-soliton S-MLFL through Q-ML stage and beating dynamics. During both the Q-ML stage and beating dynamics, multiple pulses were observed in the laser cavity whilst only a dominant pulse will gradually develop into the stationary mode-locking pulse. Figure 2g shows the last frame retrieved from Figure 2f, and the corresponding optical spectrum is portrayed in Figure 2h. The presence of the Kelly's sidebands denotes the typical characteristic of soliton fiber laser. The close-up of the beating dynamics in Figure 2f was shown in Figure 2i with an interference pattern. This beating phenomenon was not observed by a direct measurement without incorporating the TS-DFT technique, as illustrated in Figure 2j.

In contrast to the above investigation, an additional transient bound-state was observed in the second process of forming soliton regime using a similar MLFL setup as depicted in **Figure 3**a.[7] Similar as Figure 2a, five laser spikes were observed during the raised RO and transition stages before achieving stable mode-locking stage as shown in Figure 3a with a pulse-to-pulse interval of ≈38.03 ns in Figure 3b. The period is ≈3 times longer observed in the transition stage than those presented in Figure 2a. Based on the interferogram in Figure 3c, the propagation of periodic modulation along with the wavelength denotes the typical bound-state spectral profile.[42] The RTN is denoted as 0 for convenience of reference when achieving stable mode-locking stage. Two solitons of transient bound state were generated via the beating effect at the RTN of ≈-2800. These two solitons evolve to a transient bound state manner during the transition and the bound state eventually collapse due to the increasing separation between the two solitons. The relative phase (α) between the two solitons undergoes eight abrupt changes during the RTN from -1840 to -710 as shown in Figure 3f, which are also represented by the eight circles in the interaction plane as illustrated in Figure 3d. At the RTN of ≈-1100, the relative phase develops in the opposite direction so that the rotating direction is reversed after this inflection point, as shown in Figure 3f. The Fourier transformation of the transient bound-state is depicted in Figure 3e, revealing the field autocorrelation with the evolution of bound-state solitons with two pulses.[16] The two solitons have no separation at the RTN of ≈-2800. At the RTN of ≈-1250, the two solitons start to repel from each other. As a result, one of the solitons annihilates, leaving behind the other one evolving into the stable mode-locked laser pulse inside the laser cavity.

Besides experiencing the raised RO stage, the evolution dynamics of S-MLFL can also experience the Q-switching stage with the development of four stages, including initial spontaneous noise, Q-switching stage, spectral beating stage, and finally stable mode-locking stage with the schematic diagram
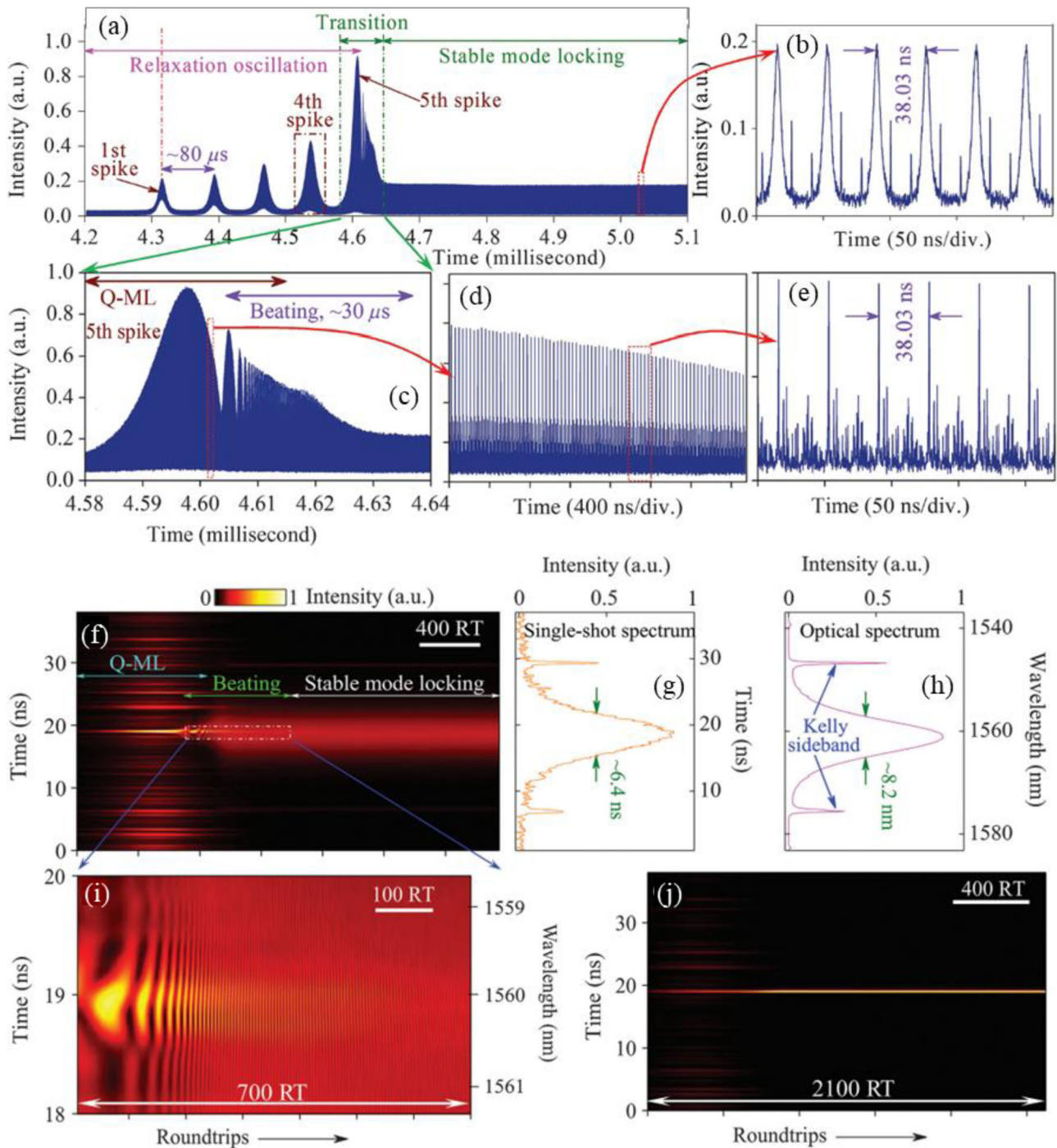
ADVANCED
SCIENCE NEWS

www.advancedsciencenews.com

LASER
& PHOTONICS
REVIEWS

www.lpr-journal.org

Figure 2. Real-time investigation of buildup and evolution dynamics in the S-MLFL. a) Experimental results measured through the TS-DFT technique and b) its spectral information of stable MLFL. c) Expanded view of the fifth laser spike in (a). d,e) Expanded views of the Q-ML in (c). f) Formation of S-MLFL from Q-ML and beating into stable mode-locking. g) Single-shot spectrum measured at the last frame in (f). h) Optical spectrum of S-MLFL measured via an optical spectrum analyzer. i) Close up of the beating dynamics in (f). j) Observation via a direct measurement without TS-DFT technique. Reproduced with permission.[7] Copyright 2019, Chinese Laser Press.

illustrated in **Figure 4**a.[43] The reason behind this difference is the integration of CNT-SA with different modulation depth and nonsaturable loss. The CNT-SA with lower modulation depth and higher nonsaturable loss results in the evolution dynamics through the Q-switching stage rather than the raised RO stage.

Therefore, a polarization independent CNT-SA with higher modulation depth and lower nonsaturable loss can suppress the unstable Q-switched lasing to reduce the buildup time in an optimized laser system.[7] The red curve in Figure 4a indicates the pumping strength increases rapidly (≈0.1 ms) and remains
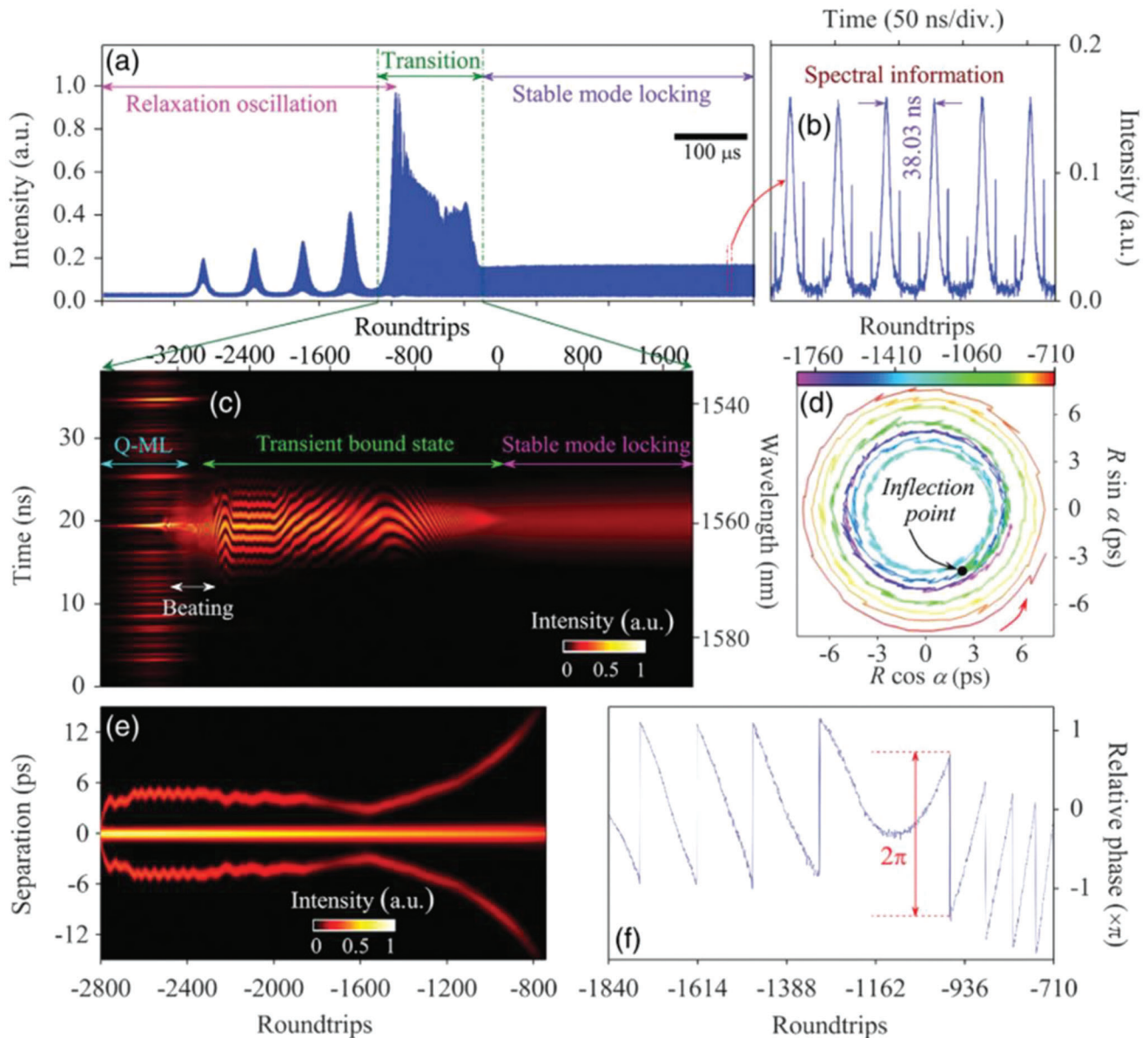
Figure 3. Real-time investigation of buildup and evolution dynamics in the S-MLFL with transient bound-state. a) Experimental results measured through the TS-DFT technique and b) its spectral information of stable MLFL. c) Interferogram revealing the evolution from Q-ML, beating, transient bound-state, and finally stable mode-locking stages. d) Dynamics of the solitons mapped in the interaction plane over 1000 roundtrips. α is the relative phase of the two solitons and R is the radius corresponds to the bound-state separation. e) Fourier transformation of transient bound-state regime over consecutive roundtrips. f) The relative phase between both solitons along with roundtrips. Reproduced with permission.[7] Copyright 2019, Chinese Laser Press.

constant afterward. As can be seen from the black curve, the Q-switched pulse is about three to four orders of magnitude longer than the mode-locked soliton. Multiple pulses coexist during the beating dynamics stage, where one dominant pulse evolves into a soliton in the stable mode-lock stage. An experimental result of the entire buildup process of laser solitons is presented in Figure 4b. The population inversion is higher in the gain medium when $0 < T_S < 6.7$ ms, where T_S is the time of spontaneous noise. In this T_S region, stimulated emission becomes dominant for the formation of Q-switched laser with pulse interval (T_Q) of 0.12 ms. Random pulsing period was

observed in the Q-switched laser pulsing with duration lasting for ≈1 min. In addition, multiple sub-nanosecond laser pulses with different peak powers coexist in the laser cavity within the beating stage. After the elimination of these multiple pulses at the end of beating stage, the dominant pulse evolves into a stationary soliton mode-locked laser with round-trip time (T_R) of ≈58.975 ns that corresponds to the laser cavity length with fundamental repetition rate of ≈16.956 MHz. An interferogram showing the buildup and evolution dynamics of stable mode-locked laser, after the Q-switching and beating stages are portrayed in Figure 4c. The x-axis indicates the time within a
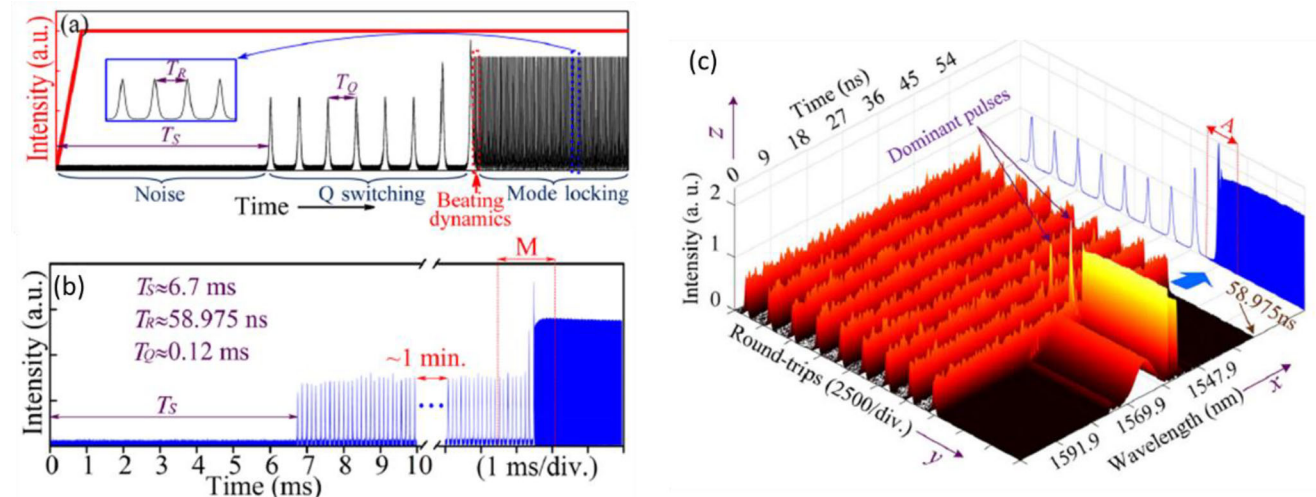
ADVANCED
SCIENCE NEWS

www.advancedsciencenews.com

LASER
& PHOTONICS
REVIEWS

www.lpr-journal.org

Figure 4. Real-time investigation of buildup and evolution dynamics in the S-MLFL experiencing Q-switching stage. a) Schematic diagram showing various transition stages from initial noise, QS pulse, beating dynamics to stable mode-lock soliton. b) Experimental results of the entire evolution process of S-MLFL. c) Real-time interferogram in the transition phase, corresponding to the time interval "M" in (b). Reproduced with permission.[43] Copyright 2019, American Physical Society.
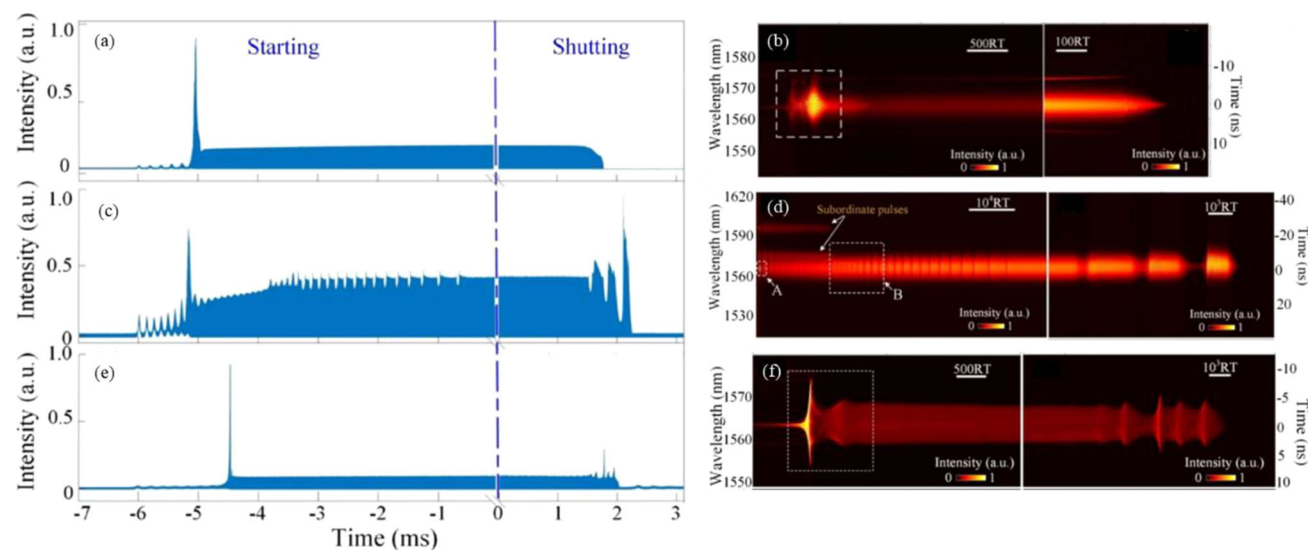

Figure 5. Real-time observation and spectral evolution dynamics. a,b) Soliton, c,d) stretched pulse, and e,f) dissipative soliton. Reproduced with permission.[44] Copyright 2019, Chinese Laser Press.

single round-trip from 0 to 58.975 ns, whereas the *y*-axis encloses the entire buildup and evolution process from spontaneous noise to stable S-MLFL across consecutive roundtrips. A theoretical model showing the beating dynamics relating to multiple pulses based on generalized NLSE was numerically simulated.[43]

Apart from CNT-SA, the buildup and evolution dynamics of S-MLFL was reported using semiconductor saturable absorber mirror (SESAM), which also experiences Q-ML stage prior to the final stable mode-locking stage.[28] This observation matches the tendency like those reported previously by Liu et al.[43] A sliding fringe pattern was observed in the transient stage between the interval of Q-switching and stable mode-locking. In the stable

mode-locking stage, temporally separated pulses with different relative phases were observed. Nevertheless, only the dominant pulse with the highest intensity survives and finally forms the stable S-MLFL.

Besides the birth and evolution process of stable S-MLFL, the investigation into extinction dynamics is also an important study. The real-time investigation of the birth and extinction dynamics in a single-walled carbon nanotube saturable absorber (SWCNT-SA) integrated S-MLFL was conducted with a net GVD of ≈−0.2 ps² as presented in **Figure 5**a.[44] The birth stage starts with the generation of a strong Q-ML laser spike and the raised RO lasts for ≈1 ms. After the raised RO stage, the S-MLFL experiences
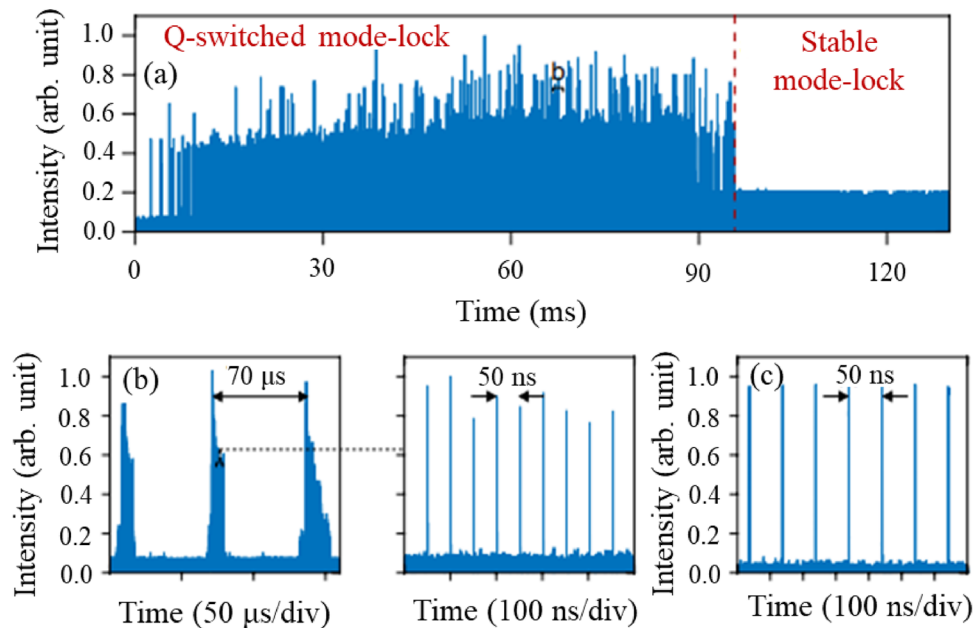
Figure 6. Investigation of the transient laser dynamics in DS-MLFL through direct photodetector measurement. a) Observation of Q-ML stage before stable mode-locking stage over a period of ≈100 ms. b) Record of Q-ML stage from region b in (a) over 2.6 million roundtrips. Q-ML consists of transient burst of temporal width ≈10 µs, which was separated by 70 µs. The expanded view shows unstable ML pulses were generated with an ≈50 ns period under each burst. c) Stable mode-locking stage with regular pulse train. Reproduced with permission.[50] Copyright 2018, Springer Nature.

beating dynamics before achieving the stable mode-locking stage. When the laser pump was turned off, the S-MLFL pulses last for ≈0.3 ms and then vanish rapidly due to exponentially increased loss of the SWCNT-SA. However, when the turn-off time is several milliseconds longer than the relaxation time of gain fiber, i.e., ≈1.5 ms, the lasing spike can be observed again after ≈1.5 ms, which is due to the accumulation process of population inversion. After this lasing spike, the gain is less than the intracavity loss, thus leading to the fluctuation and eventually annihilation of laser. The fluctuation can be reduced or even suppressed completely, with a faster turn-off time and suitable laser cavity design. A similar extinction dynamic of S-MLFL was observed, which reveals that the extinction process could be speeded up by blocking the pump power at a faster speed.[45] Figure 5b illustrates the real-time spectral evolution dynamics for the birth and extinction of a soliton. The white box indicates the beating dynamics where the strong Q-ML laser spike occurs prior to the formation of stable mode-lock laser stage. During the extinction process, the Kelly's sidebands of the S-MLFL start to be evaded and finally the central peak was extinguished.

3.1.2. Dissipative Soliton (DS)

The dissipative soliton operates in the normal dispersion regime, leading to high pulse energy generation in fiber laser cavities.[46] The dissipative effects in the dissipative soliton lead to considerably complex dynamics.[47,48] During the formation of DS in MLFL, a largely chirped pulses in the normal dispersion region exhibit rectangular profile with sharp edges.[49] Prior to the formation of stable mode-lock laser, two sharp spectral peaks with oscillating structures were observed on both edges of the pulse

spectrum. Therefore, an investigation into the buildup and evolution dynamics of DS-MLFL is important to understand its underlying features and mechanisms. The DS-MLFL was studied in an EDFL integrated with both NPR method and CNT-SA.[49] The evolution trajectory of the DS-MLFL is quite similar to the S-MLFL, which shows the evolution from raised RO stage, and the dominant peak with the highest intensity undergoes the some beating process and eventually forms the stable mode-locking stage.[44] A major difference between DS-MLFL and S-MLFL is that the highest structured spectral spikes spread along both edges for DS, whereas the highest spectral components with strong spectral oscillation are located at the central part of mode-locked soliton during the buildup process. Moreover, the high amplitude waves were observed during the buildup process of the DS-MLFL, which marks the difference from the S-MLFL.

Figure 6 shows the transient laser dynamics in the DS-MLFL generated via direct photodetector measurement.[50] Figure 6a shows a time window of 130 ms, which corresponds to 2.6 million cavity roundtrips to observe the evolution of DS-MLFL. A transient time of ≈100 ms was observed with the Q-ML operation prior to the formation of stable mode-locking stage. By viewing the region "b" from the Q-ML stage, a series of transient burst with a temporal width of ≈10 µs separated by a ≈70 µs period was observed, as plotted in Figure 6b. The expanded view in Figure 6b reveals an irregular mode-locked pulse train under each burst, which confirms the Q-ML characteristic. A stable mode-locked pulse train is shown in Figure 6c, which illustrates a regular pulse train of constant intensity. The measurement was done directly with a photodetector. Hence, even with a detection bandwidth of 30 GHz, the temporal width of the pulses recorded by the photodetector is ≈30 ps, precluding any detailed study of the underlying soliton dynamics in the transient regime.
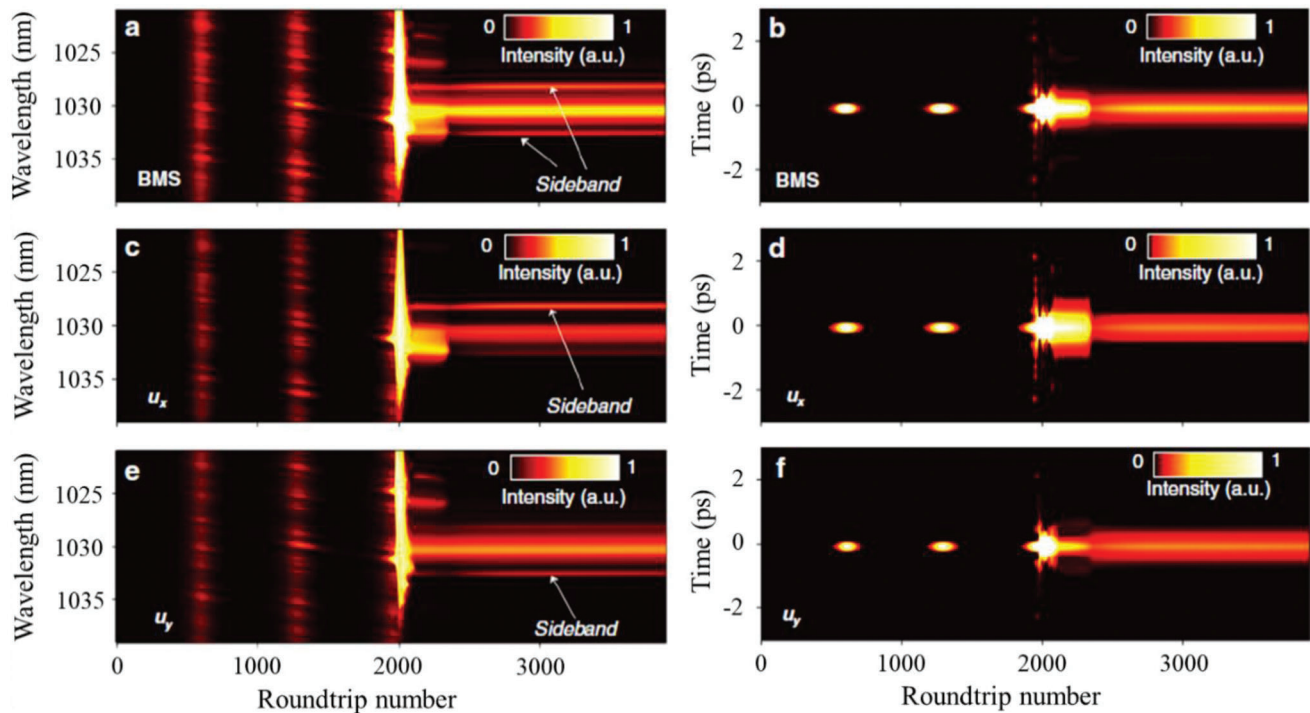
Figure 7. Real-time investigation of buildup and evolution dynamics in an almost chirped free DS-MLFL using PMF. Spectral and field autocorrelation evolutions for a,b) BMS, c,d) U_x component, and e,f) U_y component. Reproduced with permission.[55] Copyright 2022, Springer Nature.

Therefore, the TS-DFT technique is powerful tool to reveal a complete buildup and evolution process of the transient soliton dynamics in the DS-MLFL.

During the buildup and evolution process of a DS-MLFL integrated with a SWCNT-SA, spectral broadening and breathing behavior of transient dissipative structures were generated asynchronously.[51] For pump powers between single-soliton and multisoliton mode-locking regimes, the generation of mutually ignited transient solitons transforms the energy in a quantized manner along the soliton propagation.[52] Subsequently, the evolution dynamics of DS-MLFL experiences energy quantization, SPM-induced spectral broadening, and Raman soliton self-frequency shifting, thus leading to the generation of oscillations and breathing spectral peaks. Furthermore, the real-time investigation of the buildup and evolution dynamics in the DS-MLFL was also reported in a mode-locked YDFL with a net normal GVD of 0.056 ps² using the NPR technique.[53,54] The entire buildup and evolution process includes four stages, i.e., raised RO, spectral broadening, transient chaotic state, and finally stable DS-MLFL state.

An almost chirped-free DS-MLFL was designed with a hybrid-structured all-normal dispersion ytterbium-doped laser cavity consisting of a few meters of polarization maintaining fiber (PMF).[55] A phase matching principle is followed, which implements the birefringence, normal dispersion, and nonlinear effects in order to achieve the periodic boundary condition of the fiber laser. The phase matching principle confines the broadening of the spectrum by self-phase modulation and saturable absorption that compress the pulse in normal dispersion regime. This unique pulse type is termed as the birefringence man-

aged soliton (BMS), which emphasizes the role of PMF in self-consistent evolution. The two orthogonal polarized, slow (U_x) and fast (U_y) components of the PMF were also investigated for certain polarization states, in addition to the BMS. When a pulse circulates in the resonator, the coupling condition between SMF to PMF should be considered. For a certain polarization orientation (θ), two orthogonal-polarized components along the slow (U_s) and fast axis (U_f) can be expressed as

$$U_s = U_x \cos\theta - U_y\sin\theta \qquad (7)$$

$$U_f = U_x \sin\theta + U_y\cos\theta \qquad (8)$$

Without loss of generality, at the output terminal of the PMF, the U_s and U_f components are considered to translate into U_x and U_y components along the SMF, respectively. The buildup and evolution dynamics for the almost chirped-free DS-MLFL in terms of BMS, U_x and U_y components were measured through the TS-DFT technique as portrayed in **Figure 7**a,c,e, whereas their field autocorrelations are depicted in Figure 7b,d,f, respectively. The initial stage for all components experiences raised RO and beating stages, prior to the spectral broadening where parts of the soliton energy are transferred to the spectral edge thus forming sidebands. Three laser spikes were generated during the raised RO stage at ≈600, ≈1250, and ≈1900 roundtrips, whilst the beating patterns were observed from ≈2000 to 2400 roundtrips. The DS-MLFL achieves the steady state at above ≈2400 roundtrips. Both U_x and U_y display a similar evolution track to the BMS but with asymmetrical spectral sidebands, where sidebands at longer wavelength were observed for the U_y component, and vice versa.
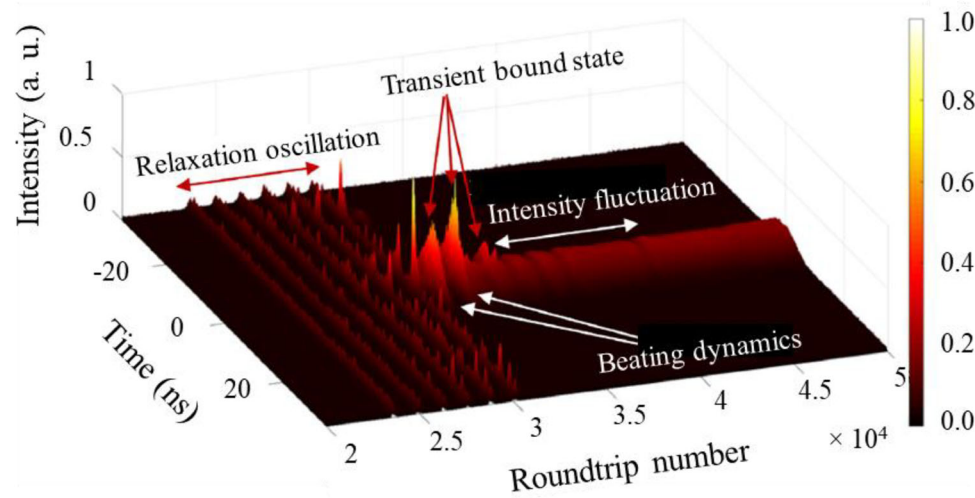
Figure 8. Real-time interferogram showing the buildup and evolution process of stable SP-MLFL integrated with a CNT-SA. Reproduced with permission.[59] Copyright 2019, Elsevier.

Apart from the birth and evolution dynamics, the real-time investigation of the extinction dynamics in an SWCNT-SA integrated DS-MLFL was performed with a net GVD of ≈ 0.02 ps^2 as presented in Figure 5e.[44] The initial stage is similar to S-MLFL but with a stronger lasing spike prior to the stable mode-locking stage. This may be owing to the shorter cavity length and higher pump power in the DS-MLFL than in the S-MLFL. For instance, the raised RO stage lasts for ≈ 1.5 ms before achieving stable mode-locking stage, whose characteristics are determined by the cavity structure and pump power. In contrast to the MLFL working in the stretched pulse regime, the shutting process of DS-MLFL experiences obvious intensity fluctuations but exhibiting a different evolution intensity envelope due to the different pulse energy, pulse width, and evolution trace. Figure 5f illustrates the spectral evolution for the starting and shutting dynamics for DS in conjunction to Figure 5e. The spectra broaden in a short time along with huge increase of intracavity energy, whereas some interference fringes were observed. Both edges have clear fringes that were generated due to the large pulse energy of the DS. Next, the spectral width undergoes broadening and compression along with the rise and fall of energy, which eventually forms a stable DS. During the extinction process of the DS, the spectral width and intensity of DS shows oscillation due to the variation in the gain. The remaining population inversion can still offer gain within the relaxation time of activator ions, but it is difficult to support stable operation.

3.1.3. Stretched Pulse (SP)

The SP, or so-called dispersion-managed soliton, is a technique that is capable of achieving pulse duration shorter than 100 fs in MLFL with a net GVD of approximately zero.[56,57] The dispersion management with fiber span of alternating dispersion contributes to the periodical stretching and recompression of the laser pulses during every cavity roundtrip.[58] A real-time investigation for the entire evolution dynamics of forming a sta-

ble SP-MLFL integrated with CNT-SA at net intracavity GVD of -0.019 ps^2 is depicted in **Figure 8**.[59] Similar to S-MLFL and DS-MLFL, the buildup process of SP-MLFL experiences raised RO stage that consists of six laser spikes with approximate intervals, and evolution stage including transient bound stage and beating stage. Nonlinear phase shift is accumulated in the laser cavity during pulse propagation, whilst the excessive accumulation of this nonlinear phase shift causes wave-breaking and other instabilities, i.e., transient bound stage.[60] The propagated pulse will adjust itself due to redundant pump power to match the laser cavity parameters, i.e., pump power, dispersion, nonlinearity, gain, loss, etc. prior to the formation of stable SP-MLFL. Therefore, the intensity fluctuation was observed owing to these complex interactions before a stable SP-MLFL was generated at $\approx 4 \times 10^4$ roundtrips.

Apart from the above work, another real-time investigation of the buildup and evolution dynamics in SP-MLFL was studied with the integration of the NPR method in the laser cavity at a net GVD of ≈ -0.007 ps^2.[61] The real-time spectral interferogram was measured by stretching the MLFL pulses across a 5 km SMF with a dispersion of 18 ps (nm km)$^{-1}$ at 1550 nm. Subsequently, the MLFL pulses were attenuated before the TS-DFT system to avoid nonlinear effects in the SMF. Instead of experiencing raised RO stage, a giant burst containing bunches of Q-switching clusters was generated during the initial stage as shown in **Figure 9**a. Based on these giant bursts, each inconsistent amounts of cluster consists of numerous transient Q-switching signals. Subsequently, each Q-switching signal is very unstable with pulse cluster duration (t_1) of ≈ 3.1 μs and the pulse cluster-to-cluster interval (t_2) lasts for ≈ 3.5 μs before reaching the final cluster at ≈ 73 μs. After ≈ 73 μs, these Q-switched signals generate a relatively long-lasting Q-ML signal from ≈ 73 to 90 μs. The dashed box in Figure 9a is enlarged in Figure 9b, prior to the formation of stable SP-MLFL at the period of ≈ 90 μs.

Apart from the birth and evolution trajectories, the real-time investigation of the birth and extinction dynamics in an SWCNT-SA integrated SP-MLFL was conducted with a net GVD of
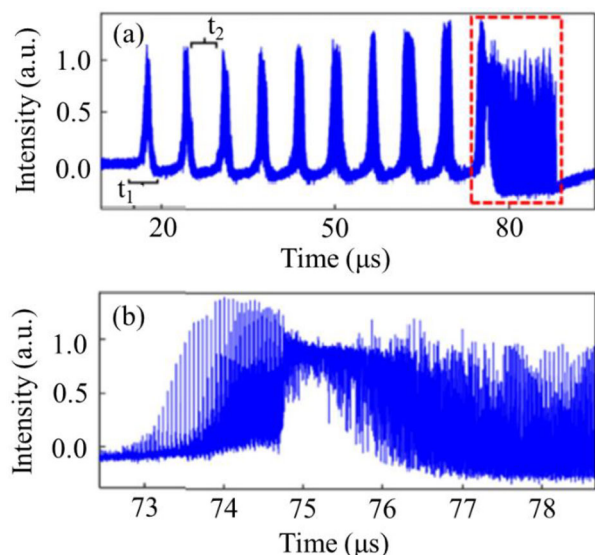
**ADVANCED
SCIENCE NEWS**
www.advancedsciencenews.com

LASER
& PHOTONICS
REVIEWS

www.lpr-journal.org

Figure 9. Real-time investigation of buildup and evolution dynamics in the SP-MLFL. a) Time trace of pulse cluster and b) expanded view of dashed box in (a). Reproduced with permission.[61] Copyright 2019, Optica.

≈ -0.004 ps^2 as presented in Figure 5c.[44] The initial stage takes ≈ 1 ms, whereas the raised RO and beating stages experience a duration of ≈ 0.8 and ≈ 0.2 ms, respectively. After the beating stage, periodic intensity fluctuation lasts for ≈ 4.5 ms where this modulation is caused by the raised RO.[31] In contrast to the S-MLFL, the instability in the SP-MLFL requires a longer time to settle down. This is because the intensity of the SP-MLFL is modulated more intensively before the annihilation of laser pulses. When the laser pump is turned off, the loss of the SWCNT-SA is exponentially increased. At the time when intracavity loss is higher than gain, an abrupt decrease in intracavity energy happens. Nonetheless, the successive pump power could still provide the accumulation of population inversion, which provides larger gain and loss again after a period of time, leading to the increase of intracavity energy. This process is similar to the Q-switching regime. Figure 5d shows the evolution dynamics of the SP-MLFL. The evolving SP is observed together with two subordinate pulses which were generated via beating dynamics. An obvious periodical modulation is observed along the roundtrip, even for the subordinate pulses. The periodical modulation starts from the RO stage (White Box A), evolves continuously (White Box B) and eventually forms a stable SP. The modulation stems from the gain variation induced by the RO stage. Upon the extinction process of the SP, the spectral width and intensity change in an unstable operation manner due to the drastic change in population inversion.

A comparison of S-, DS-, and SP-MLFLs was made in terms of its birth and extinction process. The birth stage of S- and DS-MLFLs is quite similar, the DS-MLFL has a stronger lasing spike and longer raised RO time before achieving stable mode-locking stage. On the other hand, there is an additional beating stage between RO and stable mode-locking stage during the evolution process of the S-MLFL. For the SP-MLFL, the birth stage is different from both S- and DS-MLFLs. The birth stage of the SP-MLFL does not start with a strong lasing spike but from the raised RO

and beating stages. After the beating stage, a periodic intensity fluctuation was observed. For the extinction process, the S-MLFL shows the fastest turn-off time. Both DS- and SP-MLFL experience intensity fluctuations during the shutting process, where the DS-MLFL has more obvious fluctuation with a larger evolution intensity envelope.

3.1.4. Soliton Similariton (SS)

The SS-MLFL exhibits small value of normal GVD with a parabolic temporal profile and linear chirp, whereas both temporal and spectral widths evolve exponentially.[62] The investigation of an SS-MLFL was carried out with various dynamical instabilities, i.e., formation dynamics of the laser pulse, chaotic evolution, and oscillation in the relative phase of bound-state molecules.[63] Although the soliton similariton is considered as a robust class of optical fiber laser,[64] instability regime, i.e., soliton explosion, chaos, and intermittence, was still reported, which are the universal features of DS systems existing in the transition from noise to stable MLFL.[65] In a DS system, the evolution dynamics of SS-MLFL was studied in an NPR-integrated YDFL through the TS-DFT technique.[66] The buildup and evolution dynamics of the SS-MLFL experience RO stage, transient stage (spectral broadening and spectral breathing), and finally stable stage. The behavior of pulse evolution is totally different when the parameters were modified in the laser cavity. Therefore, the SS-MLFL exhibits distinctive evolution, i.e., in different intracavity GVD regimes. In contrast to S-, DS-, and SP-MLFLs, 14 laser spikes with approximate intervals of ≈ 12 μs and random intensities were generated for the SS-MLFL in the RO stage. Apart from the birth and evolution dynamics, the extinction process of the SS-MLFL was also observed by turning off the laser pump after the stable mode-locking stage.[66] During the extinction process, three regimes were recorded, including an unstable time period, a high spectral peak over the spectrum and then a damped relaxation oscillation. When the laser pump was turned off, the laser cavity becomes unstable, leading to highly chaotic laser pulses. However, the stable mode-locking stage could be recovered after a short time owing to the residue energy stored in the gain medium. Finally, the pulse intensity starts to decrease and the laser pulse was annihilated due to the depletion of population inversion in the gain medium.

3.2. Types of MLFL

Apart from monitoring the birth, evolution, and extinction stages of these solitons, several techniques were proposed to realize certain MLFL performances. For instance, harmonic mode-locking (HML) was demonstrated to achieve higher repetition rate with respect to multiple times of the fundamental repetition rate without reducing the intracavity length. Bidirectional MLFL generates both clockwise and counterclockwise laser channels. Here, the real-time investigation of buildup and evolution dynamics was studied in both HML and bidirectional MLFLs.

3.2.1. HML

HML exhibits stable and controllable time-domain characteristics, which is an effective method to achieve high repetition rate

in MLFL.[67–69] A variety of theoretical models can be used to explain the formation mechanism of HML, such as time-dependent gain saturation effect, refractive index acousto-optic modulation effect,[70] and global soliton interaction.[71] HML presents an equal distribution of pulse interval in the time domain. By increasing the HML order, the pulse interval and repetition rate will be decreased and increased by the multiple of an integer, respectively. Therefore, high pulse repetition rate is feasible by incorporating the HML scheme, where the investigation of the real-time buildup and evolution dynamics is important to understand the underlying features and mechanisms of an HML laser. The real-time measurement of buildup and evolution dynamics in a fifth-order HML with fundamental repetition rate of $\approx$8.5 MHz was investigated through the TS-DFT technique.[72] **Figure 10**a shows the entire process for the formation of a stable fifth-order HML, which reveals its evolution from spontaneous noise to single-pulse mode-locking and eventually achieve stable HML. At $\approx 1.06 \times 10^5$ roundtrips, a big corner was observed where low peak power was generated after this corner thus leading to faster pulse velocity due to relatively lower refractive index. At $\approx 8.2 \times 10^5$ roundtrips, $\approx$5 min interval was experienced by a single laser pulse prior to the separation into five pulses at fifth-order HML within roundtrip time of 117.3 ns. The Kelly's sidebands shown in the inset of Figure 10a indicate the S-MLFL regimes. Figure 10b shows the build-up process prior to the birth of single pulse at the big corner. Both raised RO and beating stages were observed, where the expanded view of the beating stage reveals the interference pattern as enclosed in Figure 10c. After the build-up process, the evolution of HML experiences several stages, i.e., birth of a single pulse, SPM-induced instability, pulse splitting, and eventually repulsion and separation of multiple pulses as shown in Figure 10d. A conceptual representation of different stages during the entire buildup process of the HML state, including several nonlinear phenomena and ultrafast processes is shown in Figure 10e. The spectral profiles were modulated before the big corner and cleaned after the big corner, respectively. From numerical simulation,[72] the pulse interaction includes three factors, i.e., nonsoliton component such as dispersive or continuous waves in the laser cavity,[73,74] gain depletion and recovery,[75,76] and acoustic resonance[71,77] for the HML buildup and evolution dynamics during its early, middle, and later stages, respectively.

Furthermore, the HML was also presented in a mode-locked EDFL cavity integrated using SESAM with a shorter cavity length that generates fundamental repetition rate of $\approx$100 MHz.[78] It is expected that different SA could contribute to different buildup and evolution dynamics in the HML. In contrast to the investigation by Liu et al.,[72] a fourth-order HML was investigated through the TS-DFT technique, which experiences different evolution dynamics through four stages including self-starting of fiber laser, giant pulse burst (Q-ML), transient state ML state, and finally stable HML state. Apart from the conventional HML dynamics, the investigation into real-time buildup and evolution dynamics between consecutive multiple-pulsing states in a mode-locked EDFL integrated with SWCNT-SA at fundamental repetition rate of 44.1 MHz.[79] The double-pulsing and multipulsing states were generated at the pump powers of 62 and 90 mW, respectively. The transition from a double-pulse state to second-order HML could be achieved by slightly reducing the pump power up to 70 mW. A strong laser spike intensity was observed at the pump power

of $\approx$69.7 mW, which corresponds to the birth of a new pulse at $\approx$350 000 roundtrips, while the other two original pulses in the double-pulsing state exhibit an energy value close to their steady-state value. The new pulse is generated from the dispersive wave that was modulated into a narrowband pulse, which is not from the splitting of the oscillating pulses in the laser cavity. The generation of this new pulse is different from the pulse splitting process, which was developed from a single pulse.[72]

3.2.2. Bidirectional MLFL

Bidirectional MLFL exhibits the laser signal that propagates bidirectionally in the laser cavity, which is a suitable light source for dual-comb generation and application,[80–82] such as the recent demonstration of 100 and 30 GHz ultrahigh repetition-rates in bidirectional MLFL.[83] The interaction and the collision of the two pulse trains occur in every roundtrip, thus offering a special and excellent platform to explore the complex dynamics of bidirectional MLFL. The evolution dynamics of bidirectional MLFL is strongly influenced by the net GVD of the laser cavity.[84] For instance, similar dynamics in terms of spectral and temporal characteristics were observed during the buildup and evolution process of bidirectional MLFL in the net normal GVD regime through common gain and loss modulation.[85] On the other hand, independent dynamics were experienced by the counter-propagating pulses during the buildup and evolution process of bidirectional MLFL in net anomalous GVD regime.[86] Apart from the influence of net cavity GVD, the investigation into the mutually induced soliton polarization instability was performed in a bidirectional MLFL, revealing the similar periodic polarization switching behavior with a transition state of polarization rotation.[87] The soliton maintains the initial quasi-polarization-locked (QPL) state, experiences the next fast polarization rotation, and reverts into the QPL state again, thus completing the polarization switching process. Besides the net GVD and polarization switching mechanisms, bidirectional MLFL can operate in either synchronous or asynchronous mode with similar or different repetition rates.[88] A real-time investigation was performed for both synchronous and asynchronous states in a bidirectional MLFL integrated with CNT-SA operating in a net anomalous GVD of -0.069 ps^2.[89] The simultaneous synchronous and asynchronous mode-locking operations were attained by setting the appropriate pump power and adjusting the polarization state. When the polarization controller was adjusted in an intermediate state, transient switching between synchronous and asynchronous modes was observed. Based on the shot-to-shot spectral measurement, the asynchronous mode is more frequently observed than the synchronous mode. In the asynchronous mode, the clockwise and counterclockwise pulses periodically attract to and separate from each other with constant steps. Subsequently, the pulse energy gradually increases or decreases when the two laser pulses approach or walk off from each other, respectively. On the other hand, the energy of the two laser pulses always remains constant in parallel mode for synchronous mode. Besides that, the bidirectional MLFL could be switched from the asynchronous mode to the breathing synchronous mode due to the random change in gain and nonlinearity induced by the fluctuation in polarization state and pump power. This is because the
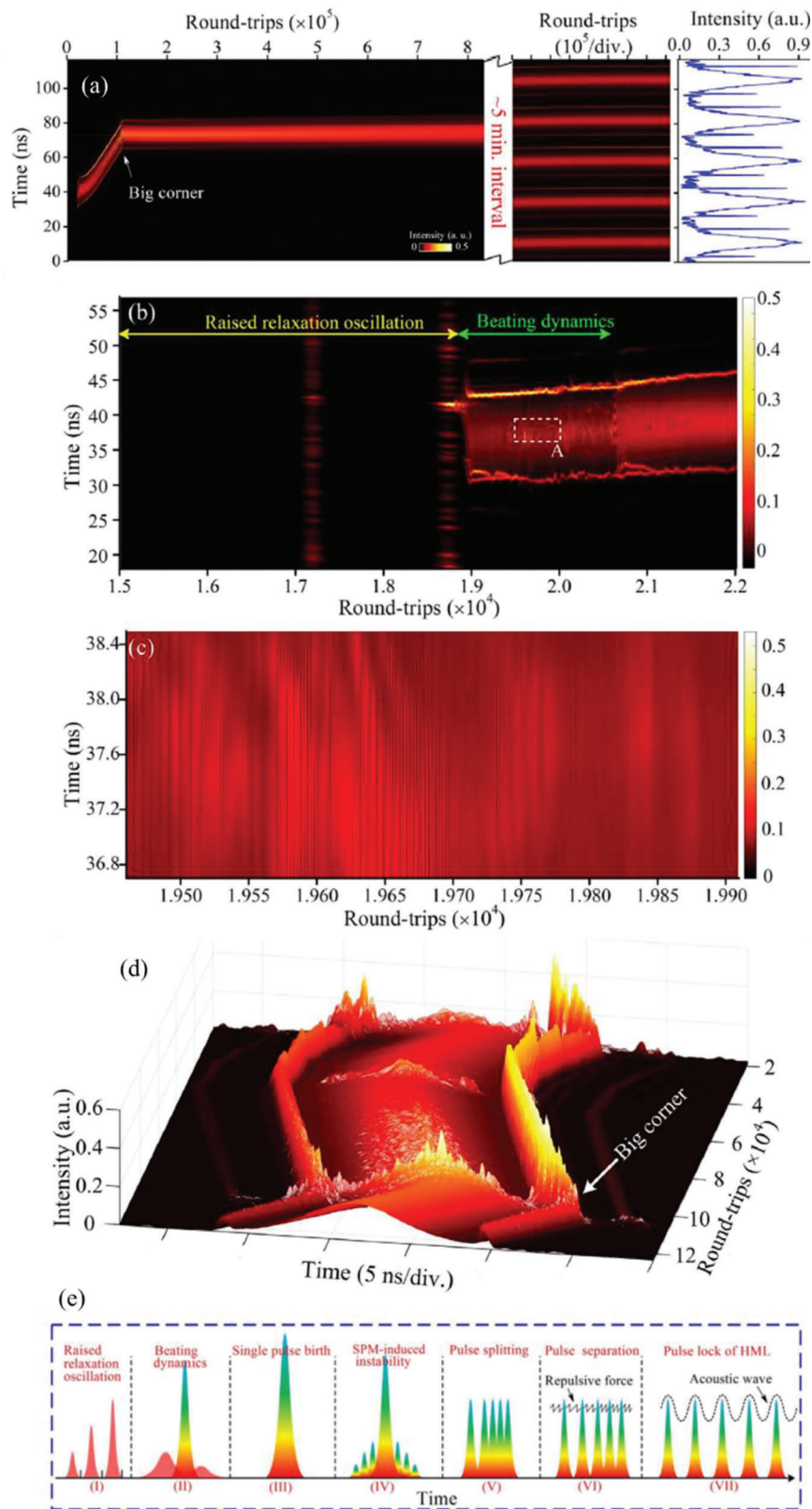
ADVANCED
SCIENCE NEWS

www.advancedsciencenews.com

**LASER
& PHOTONICS
REVIEWS**

www.lpr-journal.org

Figure 10. Real-time investigation of buildup and evolution dynamics in the fifth-order HML. a) Entire evolution process. b) Initiation stage before big corner. c) Expanded view of region A in (b). d) Evolution trajectories of HML from 1.835×10^4 to 1.23×10^5 roundtrips. e) Conceptual representation of seven stages during the buildup process of HML. Reproduced with permission.[72] Copyright 2019, Wiley-VCH GmbH & Co.

breathing solitons collide and interact in every roundtrip to exchange energy in a constant period.

Apart from integrating an SWCNT-SA, the real-time investigation of buildup and evolution dynamics in the bidirectional MLFL was also reported by using the combination of both SWCNT-SA and NPR method.[86] The bidirectional MLFL exhibits a net anomalous GVD and generates pulse durations of 570 and 790 fs for the counterclockwise and clockwise channels, respectively. The primary pulse in each channel was generated from the transition of modulation instability through two buildup stages, i.e., breathing and subordinate pulse formation into the stable soliton. The counterclockwise pulses undergo each evolution stage over a different time period, even though these pulses experience a similar evolution pattern. By contrast, the deviation in evolution matches with different pulse intensity, which contributes to the suppression of counterclockwise pulse and domination of clockwise pulse. In comparison to unidirectional soliton,[33,39] soliton molecules were not observed in both channels. This is because inelastic collision of counterpropagating pulses was formed during the formation dynamics, which shows subordinate divergent peak intensities.[90] When the intensities of these subordinate peaks achieve the threshold values, annihilation of subordinate pulses happens, leaving behind the dominant soliton pulse oscillating in the laser cavity, thus completing the entire process and achieving stable MLFL. The bidirectional MLFL in the DS regime was also employed for the investigation of complex motion dynamics in the MLFL, i.e., soliton breathing[91,92] and soliton explosion[84] in the next section.

3.3. Complex Motion Dynamics in MLFL

Apart from the generation of high repetition rate utilizing HML regime and bidirectional MLFL channels that produces both clockwise and counterclockwise laser outputs, the complex motion dynamics in MLFL, i.e., soliton molecules, soliton breathing, soliton bifurcation, soliton explosion, soliton trapping, and optical rogue wave were experimentally observed and demonstrated through the shot-to-shot measurement in real-time via the TS-DFT technique.

3.3.1. Soliton Molecules (SM)

Soliton interaction includes attraction, repulsion, and annihilation.[93] The coherent interaction of several solitons coexisting in an MLFL cavity can result in self-assembly of stable multisoliton bound states, which is also known as SM.[16,94] The SM exhibits the balance between the attractive force contributed by the GVD of bound solitons which is counteracted by the intersoliton repulsive force caused by the cross-phase modulation (XPM) effect.[95] Subsequently, two individual solitons evolve into a bound state with fixed separation and locked relative phase.[96,97] The real-time investigation of buildup and evolution process in the SM-MLFL integrated with CNT-SA was measured via the TS-DFT system.[31] The buildup and evolution dynamics of stable SM-MLFL experience five stages, i.e., raised RO stage, beating stage, transient single pulse, transient bound state, and finally the stable bound state, as depicted in **Figure 11**a. The
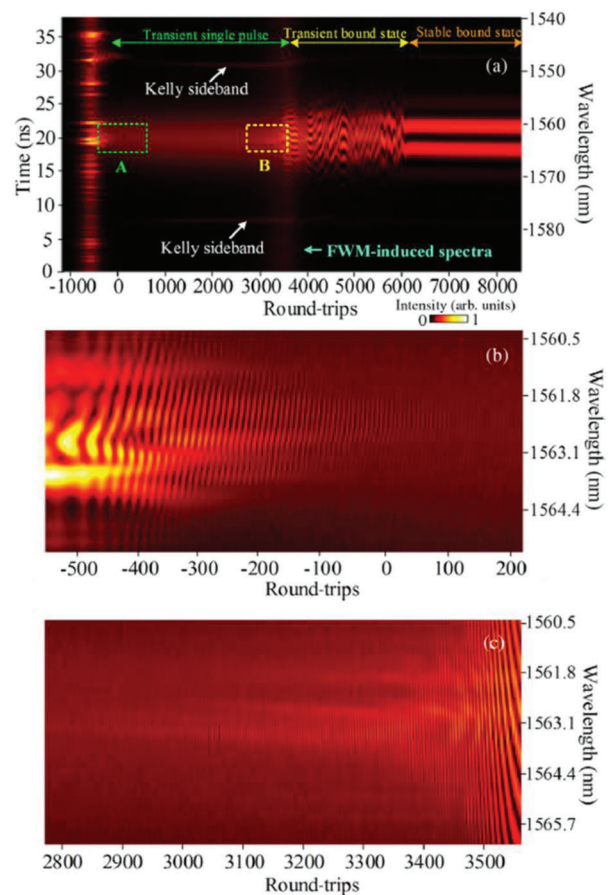

Figure 11. Real-time investigation of buildup and evolution dynamics in the SM-MLFL using CNT-SA. a) Real-time interferograms. b,c) Expanded view of dashed boxes A and B in (a), respectively. Reproduced with permission.[31] Copyright 2018, American Physical Society.

RTN was denoted as 0 upon the generation of transient single pulse. After the raised RO stage, beating behavior was observed at the beginning of the transient single pulse stage as depicted in Region A of Figure 11a or its expanded view in Figure 11b. At the RTN of 0, Kelly's sidebands were observed, which denote the MLFL works in the soliton regime. Later, the transient single pulse evolves into the transient bound state after another beating process as portrayed in Region B of Figure 11a or its expanded view in Figure 11c. Between ≈3200 and 3800 roundtrips, the broadening of laser spectra was observed owing to the spontaneous and multiple four-wave mixing (FWM) effect.[98] In particular, the FWM occurs at ≈3500 roundtrips, whereas spectral modulation arises prior to the transient bound-state. The soliton was separated into two spectra via the second beating process. In succession, the transient bound state starts where two newly generated solitons interact intensively from ≈3600 to 6000 roundtrips and a stable SM-MLFL is finally formed at ≈6000 roundtrips.

Apart from CNT-SA, the real-time investigation of buildup and evolution dynamics in SM-MLFL based on the NPR method was also characterized via the TS-DFT technique.[97] The formation of SM-MLFL was investigated in both ground and excited states.
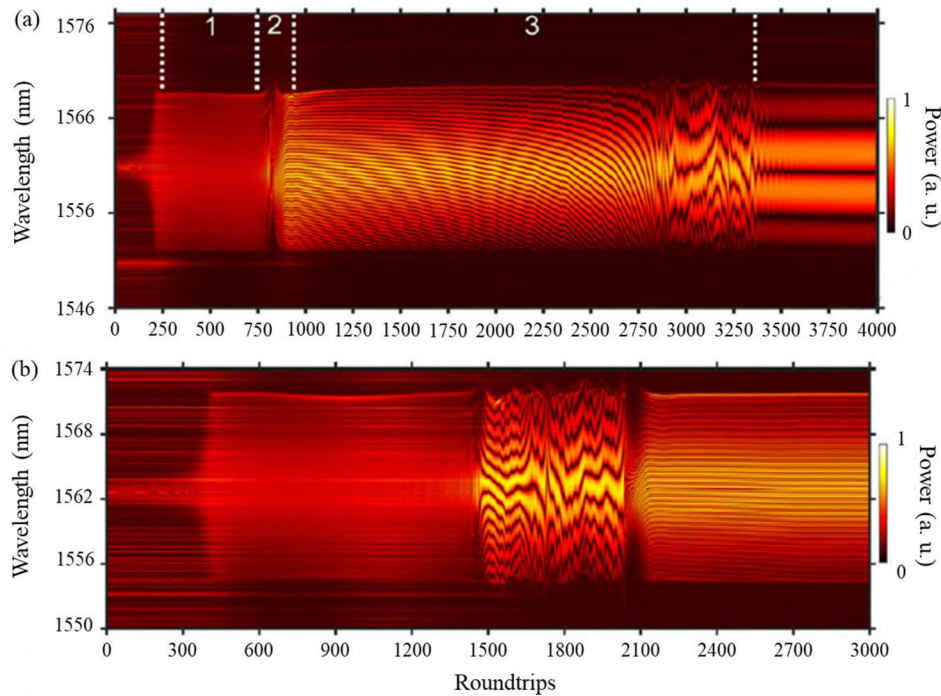
**ADVANCED
SCIENCE NEWS**

www.advancedsciencenews.com

**LASER
& PHOTONICS
REVIEWS**

www.lpr-journal.org

Figure 12. Real-time investigation of buildup and evolution dynamics in the SM-MLFL using the NPR method. a) Ground-state and b) excited-state SM-MLFLs. Reproduced with permission.[97] Copyright 2018, Wiley-VCH GmbH & Co.

The ground-state SM-MLFL possesses a lower energy that consists of bound solitons with a shorter separation, whereas the excited-state SM-MLFL exhibits higher energy, which comprises bound solitons with a larger separation.[99] Moreover, the effects of the polarization state in the laser cavity were investigated for both ground and excited-state SM-MLFLs. For ground-state SM-MLFL, the time separation of double solitons was measured to be 1.8 ps. The pulse separation of the SM-MLFL ($\Delta\tau$) was calculated according to its relationship with the modulation period ($\Delta\lambda_0$)[32]

$$\Delta\tau = \frac{\lambda_0^2}{(c \cdot \Delta\lambda_0)} \qquad (9)$$

where λ_0 is the center wavelength and c is the speed of light in vacuum. The interferogram in **Figure 12**a shows the evolution dynamics before the formation of the static ground-state SM-MLFL. At ≈250 roundtrips, well-defined intensity patterns were observed. The mode-locking stage starts to produce a wide-bandwidth soliton signal at ≈250 roundtrips which lasts until ≈750 roundtrips in Stage 1. At ≈750 roundtrips, double solitons were generated whilst the single peak was divided into three soliton peaks. Next, soliton repulsion occurs prior to the generation of these soliton peaks at ≈875 roundtrips in Stage 2. Then, solitons attract each other from ≈875 to 2750 roundtrips before soliton vibration occurs in Stage 3. Finally, stable SM was generated at ≈3500 roundtrips. Furthermore, the buildup and evolution dynamics of excited-state SM-MLFL is presented in Figure 12b. In contrast to ground-state SM-MLFL, the repulsive interaction in the excited-state SM-MLFL dominates the final stage of the entire process. The generation of bound solitons was predicted with the

overlapping of oscillatory tails at ≈3000 roundtrips,[100] which has been validated through experimental work.[101] Apart from stationary SM, evolving behaviors in the SM-MLFL were observed, such as the monotonically increased and decreased phase difference and pulse separation, chaotically hopping phase difference and pulse separation, and periodically flipping phase difference by adjusting the pump power and polarization states.[102]

Apart from the soliton regime, the investigation of SM-MLFL in the DS regime was also carried out in a mode-locked EDFL integrated with a polarization-dependent optical module.[103] The interferogram in **Figure 13**a shows the buildup and evolution dynamics of the stable SM-MLFL. A single soliton undergoes soliton splitting and complex multipulse evolution before the stable SM-MLFL was formed.[31,97] However, two pulses were formed directly at the initial stage of the field autocorrelation trace derived from the TS-DFT technique in Figure 13b with the absence of single soliton splitting, but the pulse experiences strong repulsion before the formation of stable SM-MLFL.[103] For instance, the formation of mode-locking was observed at ≈1600 roundtrips, where two solitons were developed from background noise with separation between these solitons at 4.3 ps. The soliton repulsion occurs at ≈540 roundtrips for two solitons leading to a stable soliton separation of 42 ps at ≈2140 roundtrips. The black line overlaid in Figure 13b indicates the energy evolution with an overshooting at ≈1600 roundtrips that characterizes the transition from soliton repulsion stage into mode-locking stage. Figure 13c displays the expanded view of the dashed rectangle in Figure 13a, suggesting a slight sliding phase in the pulse evolution while keeping temporal separation due to higher frequencies as the RTN is increased.[21,96] Figure 13d shows the corresponding temporal intensity evolution measured through photodetection.
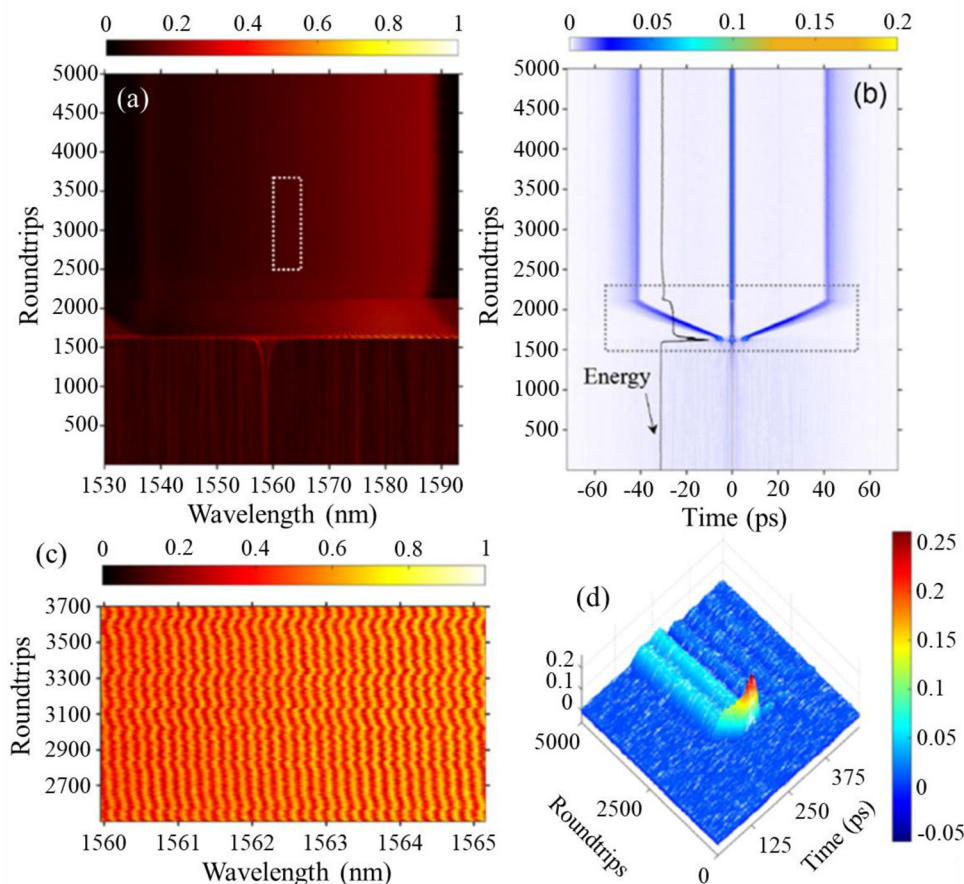
Figure 13. Real-time investigation of buildup and evolution dynamics in the SM-MLFL operating at the DS regime. a) Interferogram and b) its corresponding field autocorrelation derived from the TS-DFT technique. c) Expanded view of dashed box in (a). d) Intensity evolution of the temporal waveform. Reproduced with permission.[103] Copyright 2020, Optica.

In addition to the buildup and evolution dynamics of the SM-MLFL working at DS regime, other SM-MLFL working at the same regime was designed with net normal GVD of 0.045 and 0.0037 ps^2 in the NPR-integrated laser cavities.[104,105] According to the investigation of evolution dynamics using the TS-DFT technique in both studies, the SM-MLFL shows modulation due to the double pulsing effect whereas the position of the spectral peaks evolves quasi-periodically along consecutive roundtrips. Fourier transformation was applied and the corresponding field autocorrelation reveals the existence of three soliton peaks with a constant temporal separation. For instance, the three soliton peaks generate two pulses in field autocorrelations with pulse durations and pulse separations of ≈6 and 23 ps,[104] and ≈2.5 and ≈62.7 ps,[105] respectively. The energy was exchanged during the SM collision when noise structure appears.[106] This phenomenon was previously demonstrated for vector soliton collision.[107,108] The noise structure denotes the splitting of one or both solitons in the SM-MLFL. The moving SM along the consecutive roundtrips causes energy fluctuation and unequal intensities of the two pulses. Hence, the stronger pulse shows a higher tendency to split than the weaker pulse. Besides, an NPR-integrated mode-locked EDFL cavity was designed for the investigation of SM-MLFL in a dual-wavelength fiber laser

centered at ≈1532 and ≈1561 nm.[109] The long-wavelength SM-MLFL recovers to the initial state after soliton collision, whereas the short-wavelength SM-MLFL shows multiple intensive repulsion and attraction with energy transfer between leading and trailing soliton edges, leading to the formation of triplet SM with multiple switching behavior. In addition, both SM-MLFLs show differences in oscillating and sliding phase evolution, which indicates the multiple stabilization mechanisms of the complex DS system. In addition, the real-time investigation of the soliton collision dynamics employing a similar dual-wavelength MLFL cavity was presented.[110] Two intriguing features were observed in the spectral evolution that denotes the soliton collision, which include the spectral fringes on the main lobe and the rebuilding of Kelly's sidebands with wavelength drifting. This spectral evolution was induced by the interference dynamics between the soliton and the dispersive waves during the soliton collision process.

Apart from the NPR method, the buildup and evolution dynamics of the SM-MLFL were also investigated by integrating an SESAM into a ytterbium-doped fiber laser (YDFL) with a net normal GVD of 0.034 ps^2.[28] The pulse was initiated from a narrow spectrum to modulation instability during the birth stage. Then, the two oscillating spectral peaks were generated at ≈100 roundtrips, which achieve steady state with two fixed solitons
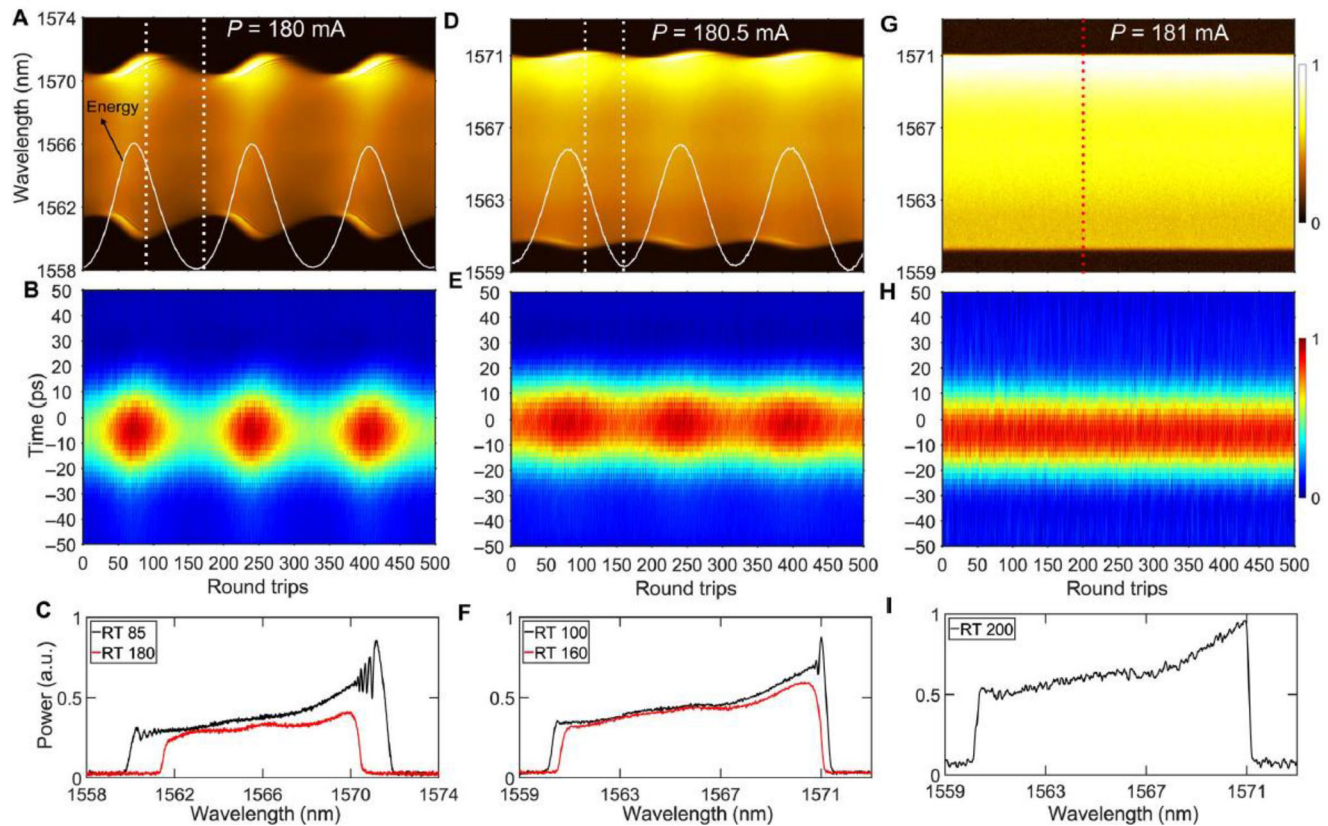
ADVANCED
SCIENCE NEWS

www.advancedsciencenews.com

LASER
& PHOTONICS
REVIEWS

www.lpr-journal.org

Figure 14. Real-time investigation of breathing dynamics in a DS-MLFL. A,D,G) Shot-to-shot measurement over 500 consecutive roundtrips with increasing pump current. B,E,H) Temporal evolution of pulse intensity over consecutive roundtrips. C,F,I) Shot-to-shot spectra recorded at the maximum and minimum roundtrips within a period. Reproduced with permission.[18] Copyright 2019, American Association for the Advancement of Science.

in the final stage. In the final stage, an oscillating and sliding fringe pattern was observed for the SM-MLFL. Besides the oscillating and sliding fringe pattern, the soliton shaking motion in the SM-MLFL was also observed in a mode-locked EDFL at a net GVD of -0.0031 ps^2 through the TS-DFT technique.[21] By setting an appropriate pump power and adjusting the polarization state of the laser cavity, soliton pairs with simplex oscillatory dynamics, shaking soliton pair with quasi-chaotic-periodically evolving phase oscillation and sliding phase dynamics were experimentally observed. Apart from the simple oscillatory dynamics, the degree of freedom of the dynamics in soliton pairs could be further explored. The interferogram in real-time measurement provides access to multifold internal dynamics. Therefore, the shaking soliton pairs were generated by the superposition of multiple oscillatory motions.[111] These oscillatory motions appear in both quasi-periodic and chaotic regimes. Moreover, the combination of different internal dynamics contributes to shaking soliton pairs with sliding phase dynamics. For instance, the gain dynamics and soliton interactions facilitate these multifold internal dynamics, governed by the subtle energy flows between each constituent.

Apart from EDFL and YDFL, the investigation of spectral evolution in soliton molecules was performed at a ≈ 1.7 μm thulium-doped fiber laser (TDFL) using the NPR method.[112] The SMF-28e can be used as the dispersive medium due to its acceptable loss at this waveband. Therefore, the TS-DFT was performed by

stretching the mode-locked laser pulse through a 10 km SMF-28e, which resolves a shot-to-shot interference pattern of the spectrum for the soliton molecule. An interference pattern of the soliton molecule is kept constant as a function of roundtrips, denoting the soliton molecule is stable without evolving phase relationship of the two solitons. Apart from soliton molecule, single and double pulse operations were also observed using a low pump power and adjusting the polarization states, respectively. This work shows possibility for the application of the TS-DFT method in other operating wavelengths than ≈ 1.06 and 1.55 μm.

3.3.2. Soliton Breathing

The soliton breathers exhibit a localized and oscillatory evolution track for energy evolution.[113] In a DS-MLFL system, soliton breathing dynamics has dynamically oscillatory behavior in contrast to the stationary DS.[18,114] Nevertheless, both breathing DS in stationary and dynamical states can form stable bound states by displaying molecular dynamics. The real-time soliton breathing dynamics were investigated with a EDFL mode-locked with the NPR method at a net normal GVD of 0.14 ps^2 through the TS-DFT technique.[18] The breathing DS could be achieved by monitoring two major factors, i.e., pump power and polarization state. The spectral and temporal evolutions of the breathing DS-MLFL over consecutive roundtrips are depicted in **Figure 14**a,b.
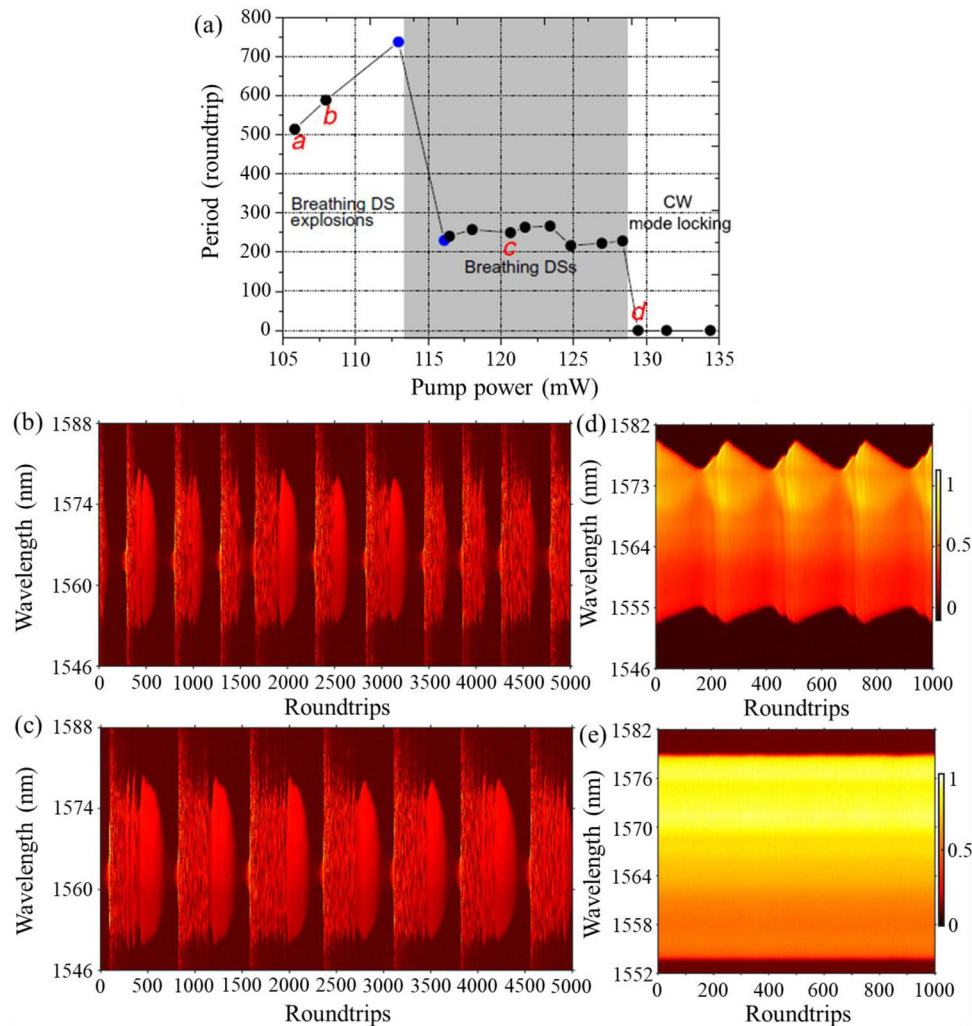
Figure 15. a) Bifurcation diagram of the breathing DS in a mode-locked EDFL. b–e) Interferogram for real-time shot-to-shot spectral information for Points a, b, c, and d in (a). Reproduced with permission.[117] Copyright 2019, American Physical Society.

According to the spectral information, compression and stretching of pulse spectrum were observed periodically within ≈170 roundtrips. The pulse evolution across consecutive roundtrips is periodic, which agrees with the observation of single and dual-soliton pulsating regimes.[115] Hence, the variation of peak intensity was observed in every period. The pulse energy is deduced by integrating the power spectral density over the entire wavelength band as depicted in the white curve of Figure 14a. The magnitude difference between the highest and the lowest energy within each period varied by ≈2 times. The pulse spectrum at the maximum and minimum roundtrips within a period is illustrated in Figure 14c. The fringes were formed at the edges of 85 roundtrips (RT-85) due to the shock wave dynamics in the DS regime.[116] The breathing ratio is defined as the ratio between the largest to the narrowest spectrum within a period.[91] The formation of a stationary DS is denoted by the breathing ratio of 1.[18] By increasing the pump power, the breathing ratios decreased from 1.35, 1.05 to ≈1 in Figure 14a,d,g, respectively.

Apart from the investigation above, the experimental measurement of the explosion of a breathing DS, prior to the formation of the breathing DS in a mode-locked EDFL cavity integrated with the NPR method, was performed at lower pump power as shown in **Figure 15**a.[117] By increasing pump power thresholds of ≈106, ≈113, and ≈128 mW, breathing DS explosion, breathing DS, and CW mode-locking stages were achieved, respectively. Figure 15b–e illustrates the dynamics of shot-to-shot spectral information, which represents Points a, b, c, and d, in Figure 15a, respectively. In the breathing DS explosion stage, a weak tendency of breathing DS instability was observed at higher pump powers across 0 to 5000 roundtrips. For the breathing DS, periodic spectral evolution was disturbed by broad and chaotic pulse spectra, denoting the explosion of breathing DS with periodic energy variation in relatively weaker and narrower spectra from 0 to 1000 roundtrips. Therefore, the breathing mechanism was not observed for the stable CW mode-locking stage.

Furthermore, the DS-MLFL operating in the soliton similariton regime was also spectrally characterized by multipulse

ADVANCED
SCIENCE NEWS

www.advancedsciencenews.com
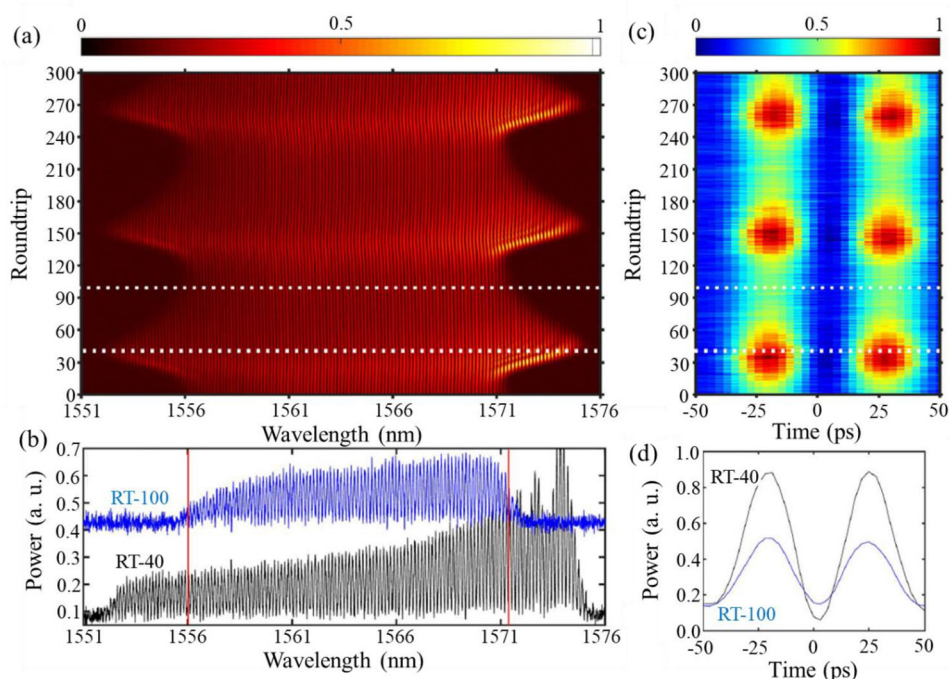
LASER
& PHOTONICS
REVIEWS

www.lpr-journal.org

Figure 16. a) Real-time investigation of breathing dynamics in the BSPMs. Shot-to-shot spectral information (a) over consecutive roundtrips and b) at RTN-40 and RTN-100. Temporal intensity profile c) over consecutive roundtrips and d) at RTN-40 and RTN-100. Reproduced with permission.[18] Copyright 2019, American Association for the Advancement of Science.

soliton complexes with breathing behavior, as revealed through the TS-DFT technique.[118] These multipulse complexes consist of two to nine circulating dissipative solitons exhibiting picosecond pulse duration with temporal separations from ≈5 to 40 ns. In addition, multipulse complexes separated by ≈40 ps coexists with multiple single pulses separated by ≈30 ns were presented for the SM-MLFL. The breathing dynamics of the multipulse complexes were observed over hundreds of roundtrips. The multipulse breather regime reveals the presence of breathing soliton molecules for the DS-MLFL operating in the soliton similariton regime.

Besides the breathing DS, real-time shot-to-shot spectral information for evolution from a stationary soliton to a pulsating soliton was reported in an S-MLFL integrated with the NPR method at a net anomalous GVD of ≈ -0.1 ps^2.[119] The intensity of the resonant Kelly's sidebands could be enhanced dramatically before the generation of soliton modulation instability by increasing the pump power. However, the soliton intensity is just slightly increased in spite of the enormously increased resonant Kelly's sidebands intensity. Therefore, the minor increase of soliton intensity leads to a huge intracavity perturbation, thus inducing phase matching to achieve soliton modulation instability owing to the interaction between soliton and dispersive waves.[120] Moreover, further increase in pump power leads to breathing S-MLFL with more chaotic parametric sidebands, dramatic multipulsing dynamics, and dispersive wave instability. For instance, the breathing S-MLFL with chaotic pulsating features was demonstrated with higher pump power and adjustable polarization states.[121]

Apart from the breathing soliton, the breathing soliton pair molecules (BSPMs) were also investigated in an SP-MLFL integrated with the NPR method at net GVD of ≈ 0.002 and -0.0031 ps^2.[18,122] The peak power clamping effect saturates the laser pulse to provide higher peak power in the SP-MLFL regime.[123] **Figure 16**a reveals the spectral information of the BSPM motion dynamics over consecutive roundtrips. The BSPM exhibits the interference pattern that is present in the typical spectra of the SM-MLFL.[16] The shot-to-shot spectra of the largest and smallest widths of the BSPM within a period at RTN-40 and RTN-100 are depicted in Figure 16b. The large periodic variations experienced by the spectral width do not influence the separation of spectral intensity peaks, which remains constant as 0.18 nm over consecutive roundtrips. Figure 16c reveals the corresponding temporal intensity profile of the BSPM over consecutive roundtrips, which exhibits a constant intramolecular temporal separation of 45 ps. From Figure 16d, the temporal intensity profiles at RTN-40 and RTN-100 shows the breathing dynamics of the BSPMs.

Apart from the conventional breathing DS, soliton, and SP, the real-time investigation of soliton breathing dynamics in breather complexes, i.e., breathing soliton molecules (BSMs) and breathing soliton pairs (BSPs) were studied in bidirectional MLFLs.[91,92] The switching dynamics in the BSMs could be triggered by saturable absorption parameters and the control of polarization states that exhibits two dynamics, i.e., constant pulse separation or strong repulsion after switching process. The collision of counterpropagating BSMs is responsible for the time-varying separations between the breathers and transient pulse splitting during the switching process. The gain depletion and
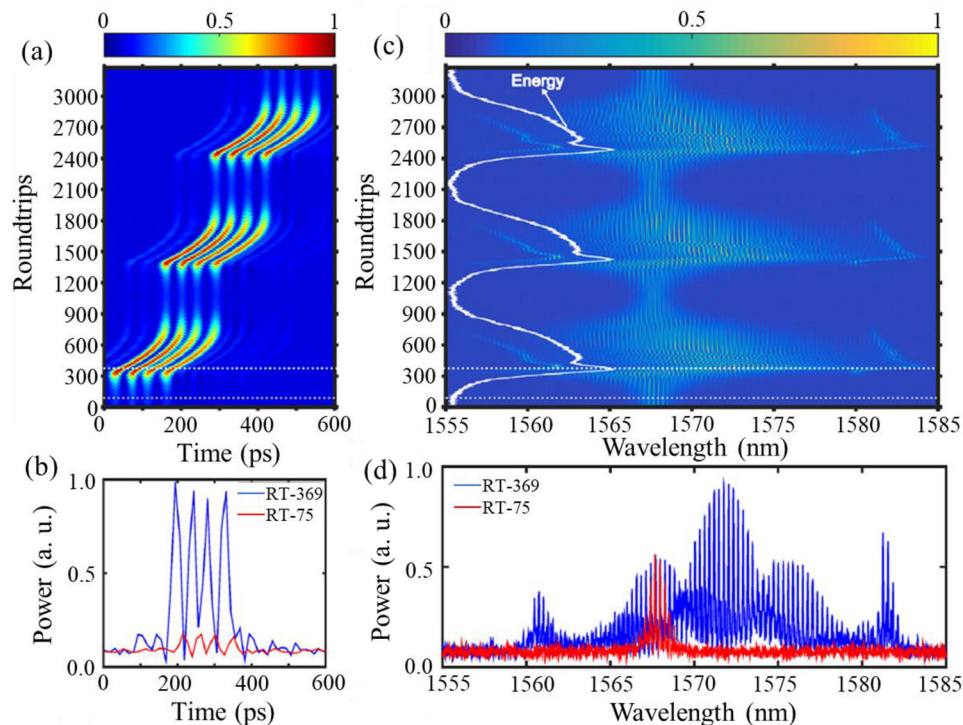
Figure 17. Real-time investigation of breathing dynamics in the BQMs. a) Temporal intensity profiles over consecutive roundtrips and at b) RT-75 and RT-369. c) Shot-to-shot spectral information over consecutive roundtrips and at d) RT-75 and RT-369. Reproduced with permission.[113] Copyright 2021, Wiley-VCH GmbH & Co.

recovery provide the intensive repulsion and transient twist of the BSM, whereas the gain and the loss dynamics play the role in the switching of the BSM. On top of that, the collision of the BSPs due to the counterpropagating breathing solitons increases the intensity of optical rogue waves, which causes the dissociation and annihilation of the BSPs in the bidirectional MLFLs. During the buildup of the BSMs, multiple single soliton explosion and instantaneous pulse splitting are its distinct features, in contrast to the BSPs with nanosecond pulse separation.

Furthermore, real-time investigation of breather-quartet molecules (BQMs) in an NPR-integrated mode-locked EDFL was studied.[113] The temporal intensity profile of the four BQMs was observed with large periodic intensity variations over ≈1000 roundtrips as portrayed in **Figure 17**a. The background with a relatively low intensity was formed by slowing decaying dispersive waves radiated by the breathers, which is important for the long-range operation of BQMs.[124,125] Nearly an order of magnitude change in the peak intensities was observed between RT-75 and RT-369 as shown in Figure 17b. According to the shot-to-shot spectral information in Figure 17c, the BQM exhibits a typical interference pattern like those present in the spectrum of the SM-MLFL.[16] The energy of the BQM indicated in the white curve in Figure 17c was deduced by the integration of power spectral density over the entire waveband, which evolves over consecutive roundtrips synchronously. The spectrum evolves periodically over consecutive roundtrips. The compression and the stretching of the pulses were observed in the vicinity where they reach the lowest and highest peak intensities, respectively. The spectral width at RT-369 is nearly eight times wider than that

at RT-75 as presented in Figure 17d. The Kelly's sidebands exhibited in the RT-369 denote the radiation of resonant dispersive waves from solitons when disrupted by lumped nonlinear losses and intracavity components in a roundtrip.[126] The periodical emission of these dispersive waves occurs during hundreds of cavity periods with synchronous oscillation at both the center wavelength and the wavelengths of Kelly's sidebands.[124] These wavelength oscillations were contributed by both dispersive waves and XPM of the BQMs. The breathing dynamics of the BQMs were numerically simulated via the NLSE, which was solved with standard symmetric split-step Fourier algorithm.[127] From the numerical result, soliton creeping behavior was observed with periodic asymmetric temporal profiles and shifting in center wavelengths during the soliton breathing process.

A recent demonstration of a fiber laser working in the breathing soliton regime shows frequency locking at Farey fractions.[128] This frequency-locked breather states are robust toward pump power and polarization variations, and breathing frequency with a narrow linewidth and a high signal-to-noise ratio. A fractal dimension of the winding numbers of breathers approaches that of devil's staircase, denoting the universal nature of a laser. Therefore, the investigation of universal dynamics in frequency locking is feasible by the demonstration of this breather mode-locked fiber laser. For instance, a universal frequency-locking process was tailored in a close-loop laser resonator via the nonlinear interaction between the cavity repetition rate provided by the laser resonator and the breathing frequency. This generates frequency-locked breathers, which have excellent stability against perturbations in pump power and polarization. Besides, dispersion is very
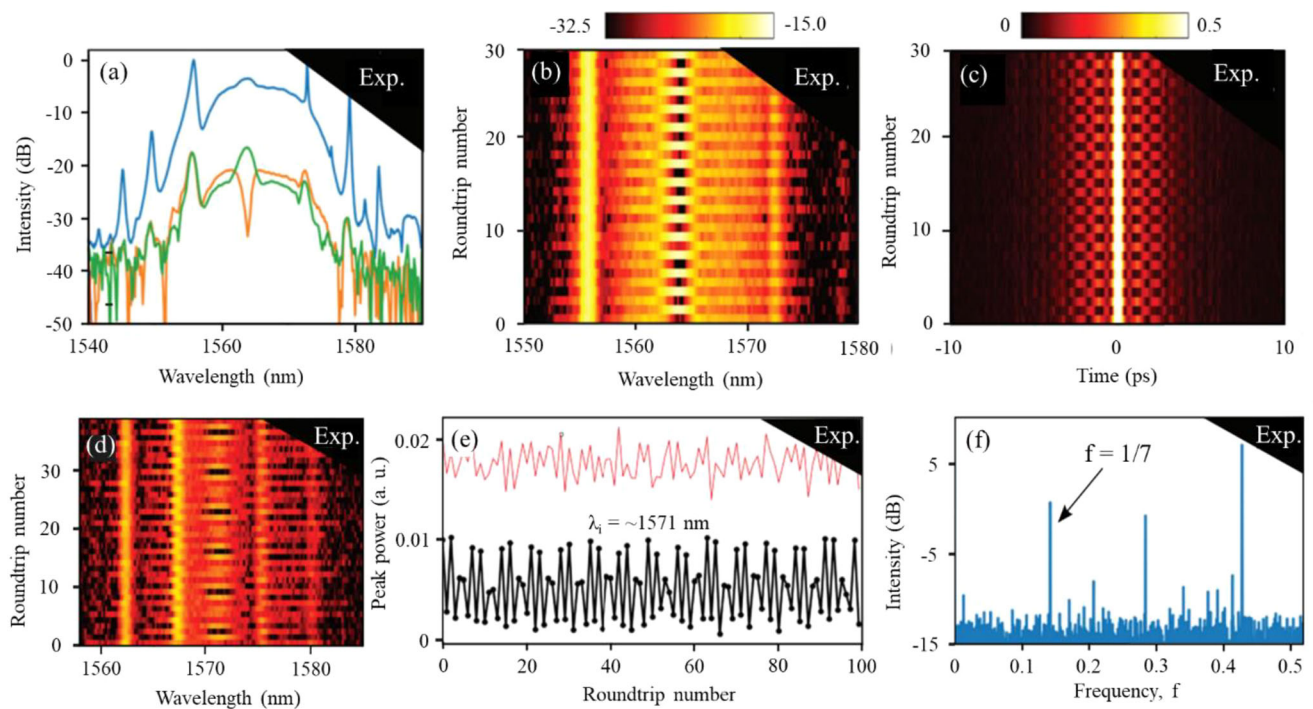
Figure 18. Period-2 solitons of a mode-locked EDFL. a) Optical spectrum (blue line) and TS-DFT spectra of two successive roundtrips (green and orange lines). b) Evolution map showing oscillation of two successive roundtrips. c) Evolution of the first-order temporal autocorrelation trace over consecutive roundtrips through Fourier transformation of the TS-DFT spectra in (b). Characterizations of multiple period oscillations in terms of d) evolution map, e) evolution of total pulse intensity (red line) and intensity close to λ_i (black line) as a function of roundtrip number, and f) Fourier transformation of intensity close to λ_i revealing periodicity of 7 roundtrips ($f = 1/7$). Reproduced with permission.[135] Copyright 2023, Wiley-VCH GmbH & Co.

important to generate frequency locking of breathers. Therefore, the laser cavity should be designed with a nearly zero net dispersion, where the frequency locking of breathers does not occur for laser operating in moderate or large normal dispersion regimes. The former dispersion regime oscillates with a period ranging from several to dozens of round trips, whilst the latter dispersion regime generally features a much longer period of the order of hundreds of round trips, indicating different underlying formation mechanisms.

3.3.3. Soliton Bifurcation

A bifurcation occurs when a major change was generated to the organization of a system due to a minor change in physical parameters. A period-doubling bifurcation (PDB) is important in a periodic system, which is being prevalent in all disciplines involving nonlinear dynamics. Hence, an investigation to the dynamics of PDB and its subsequent destabilization is essential to monitor a nonlinear system such as an MLFL dissipative oscillator. The PDB generates a periodic oscillation of the pulse parameters when monitored at a fixed soliton solution such that the laser dynamics could be qualified as a pulsating DS regime.[129–131] A pulsating solitons involve short-period pulsation (SPP), long-period pulsation (LPP), or multiple-period pulsation (MPP).[132] A major difference between SPP and LPP is the bifurcation mechanism, such that the pump power is decreased from the region of stationary mode-locking for the LPP,[18,133] whilst the SPP always occurs

beyond the stationary mode-locking region.[132,134] Moreover, the MPP reveals a complex intertwined bifucation region of the SPP and LPP.

The experimental observation of the SPP for stable period-2 pulsating solitons in an MLFL at ≈1560 nm was presented with a real-time TS-DFT measurement.[135] The MLFL was realized through the NPR method at a pump power of ≈80 mW, whereas a 1.3 km DCF was employed as the dispersive medium for the TS-DFT setup. **Figure 18**a,b reveals a period of two roundtrips for the soliton spectrum measured through the TS-DFT setup. The oscillation is observed within a narrowband near the center of the soliton spectrum, which leaves a tiny bump as a hint. Figure 18c presents the first-order autocorrelation trace obtained through the Fourier transformation of the single-shot TS-DFT spectra from Figure 18b, which shows a deformation from typical bell-shaped soliton with extended tails bearing faint oscillations. This deformation is emanated from dispersive waves, which are radiated out periodically from the soliton. The experimental observation of the LPP with period-7 pulsating solitons was observed at a pump power between 80 and 90 mW. Figure 18d shows the oscillating spectral patterns with the periodically changing center part of the optical spectrum, whilst the recurrence was observed at every 7 roundtrips. This period-7 pulsating solitons are manifested in Figure 18e, which was extracted from the TS-DFT measurement. The black line indicates the intensity close to the center wavelength (λ_i) of 1571 nm, whereas the red line denotes the total intensity of the pulse, showing a nearly constant intensity within the noise fluctuations of the oscilloscope, making an illustration
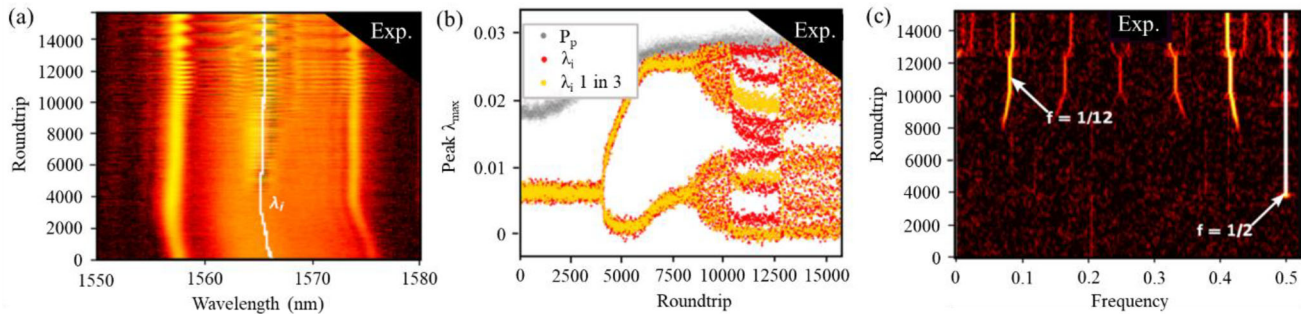
ADVANCED
SCIENCE NEWS

www.advancedsciencenews.com

LASER
& PHOTONICS
REVIEWS

www.lpr-journal.org

Figure 19. Transient dynamics of pulsating solitons under a millisecond ramp up of the pump power. a) Spectral evolution over consecutive roundtrips. b) Evolution of spectral intensity at λ_i. c) Fourier transformation of spectral intensity pulsation at λ_i. Reproduced with permission.[135] Copyright 2023, Wiley-VCH GmbH & Co.

of "invisible" pulsation. In Figure 18f, a Fourier transformation of the intensity close to the λ_i was performed on a full acquisition of 1600 roundtrips, which shows a periodicity of 7 roundtrips ($f = 1/7$).

The transient dynamics of the bifurcation sequences starting from a single-period soliton and period-N solitons were studied by increasing the pump power from 70 to 90 mW. **Figure 19**a shows the evolution map over 15 000 cavity roundtrips. To shed more light on the phenomenon and timescale at stakes, the development of the intensity in the oscillating part of the spectrum at the λ_i is presented against roundtrip number in Figure 19b. The first and second bifurcations occur at 4000 and 8000 roundtrips, which correspond to the 2-period pulsation and the starting of the modulation for the oscillation envelope, respectively. A structure emerges in the oscillation pattern between 10 500 and 12 500 cavity roundtrips, which denotes the organization of the oscillating patterns into an integer periodicity. One out of every three data points of the same acquisition was plotted in red dots, where four branches were observed, which indicate 12-periodicity. An intensity spectrogram at λ_i is presented in Figure 19c. The Fourier transformation was calculated for 1024 points of each cavity roundtrips and the evolution of the spectral density was plotted in log scale as the roundtrip number is increased. The spectral density is flat for the first 4000 roundtrips, thus denoting that the intensity at λ_i is not oscillating. The first and second bifurcations occur at ≈4000 and 8000 roundtrips, where the signal at a frequency, $f = 0.5$ appears rapidly which corresponds to the 2-period oscillations and the apparition of a signal was generated at $f = 0.08$, respectively. The spectrogram shows that the frequency continuously drifts toward higher value until $f = 1/12$. This regime corresponds to the 12-periodicity, which is presented in Figure 19b. After 12 500 roundtrips, the peak frequency drifts toward higher frequencies. The spectrogram is reproducible with a slightly different initial state, and two successive bifurcations with 14-periodicity ($f = 1/14$). Besides that, a period-2 SPP was also presented in an MLFL operating under the DS regime at a pump power of 437 mW, whereas the evolution map was recorded through the TS-DFT technique over 20 roundtrips. Period doubling was observed at the λ_i of the spectrum. The increase of pump power leads to multipulse operation and chaotic behavior, which disrupts the mode-locking operation.

3.3.4. Soliton Explosion

Akin to soliton, breathing DS exhibits explosions whereas this laser instability was attributed to nonlinearity-mediated giant Q-switching. Although stationary regimes of mode-locked fiber lasers have been utilized for practical applications, understanding the nonstationary regimes are very important as these instabilities are detrimental to applications. A deep insight into the conditions of the nonstationary regimes is important to design a system and to control laser parameters to prevent these instabilities. Therefore, the study of soliton explosion along with the breathing regime is very important to improve the stability of mode-locked lasers by considering the overlooked instability in laser design. Upon nonlinear propagation of soliton when experiencing strong energy dissipation, the sudden structural collapsed soliton is robust recurrence to the original state, in which this phenomenon is dubbed as soliton explosion.[136,137] A real-time observation of soliton explosion dynamics was conducted in an NPR-integrated mode-locked EDFL with a net normal GVD regime.[138] The pump power threshold for stable MLFL is 129 mW, whereas the soliton explosion dynamics in the MLFL was observed at the pump power threshold of 155 mW. By increasing the pump power to 157 mW, the soliton explosion process lasts for a longer time. This condition is similar to a mode-locked EDFL working in the net anomalous GVD regime. Hence, regardless of the net GVD regime, a more rigorous explosion event was typically observed at higher pump power.[139] The evolution of temporal intensity of DS-MLFL experiencing soliton explosion over consecutive roundtrips is illustrated in **Figure 20**a. Initially, the two parent pulses separated by ≈260 ps attract each other before merging into a single pulse at ≈9000 roundtrips. The representative cross-sections at 5000, 10 000, and 15 000 roundtrips are illustrated in Figure 20b. In these roundtrips, two parent pulses, merging of parent pulses and generation of the second pulse were detected. The synchronous spectra measured by the TS-DFT technique are presented in Figure 20c. From ≈9000 to 13 500 roundtrips, the pulse explosion has a broad and chaotic spectrum. Figure 20d shows the representative cross-sections at 5000, 10 000, and 15 000 roundtrips. The expanded view of the box at RT-5000 in Figure 20d is enlarged in Figure 20e. The interference pattern observed at the RT-5000 prior to the soliton explosion event indicates the two pulses are
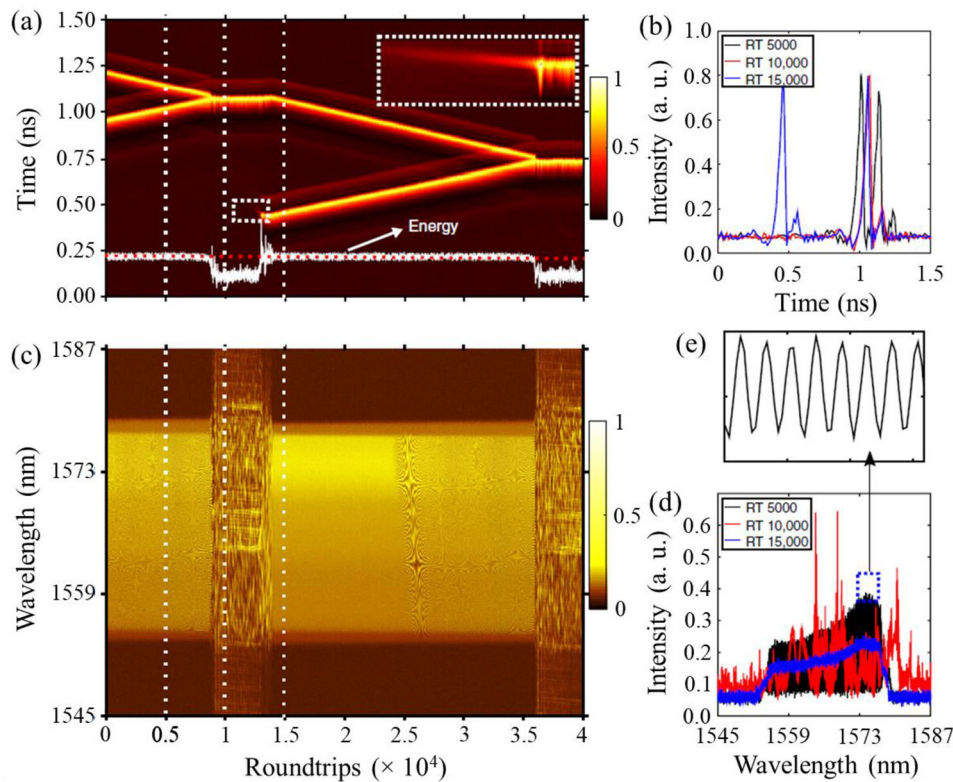
**ADVANCED
SCIENCE NEWS**

www.advancedsciencenews.com

**LASER
& PHOTONICS
REVIEWS**

www.lpr-journal.org

Figure 20. Real-time investigation of soliton explosion dynamics in a mode-locked EDFL. a) The spatiotemporal intensity evolution. b) Three representative cross-sections in (a). c) Synchronous real-time spectra evolution. d) Three representative cross-sections in (c). e) Expanded view for RT-5000. Reproduced with permission.[138] Copyright 2019, Springer Nature.

coherent.[139] Moreover, the pulse-to-pulse spectral interval of 0.063 nm corresponds to a temporal separation of 130 ps. This matches with the temporal separation of ≈124 ps for RT-5000 in Figure 20b. This soliton explosion event agrees with the mutually ignited soliton explosion phenomenon in single-soliton and multisoliton regimes.[115,140] The multisolitons interact through the transient gain response in the gain medium, thus leading to soliton explosion by the dynamic variation in the soliton energy.

The soliton explosion dynamics were also investigated in an S-MLFL at a net anomalous GVD.[139] In contrast to DS-MLFL, the Kelly's sidebands of stable S-MLFL were eliminated during the soliton explosion process, whereas the transient ordering of solitons occurs during an explosive event, thus leading to the emergence of transient soliton molecules featured by the interference fringes. These interference fringes exist only for a few hundreds of roundtrips before the spectra revert into the chaotic patterns. The soliton explosion event exhibits four features: stable MLFL, spectral collapse, destruction of Kelly's sidebands, and finally chaotic patterns. Apart from S-MLFL, the soliton explosion dynamics were also investigated in a bidirectional mode-locked EDFL cavity with the soliton breathing behavior.[84] The changing of polarization state and increasing of the pump power triggers the breathing soliton explosion during the build-up stage. In the bidirectional MLFL cavity, the time-stretched waveforms of the clockwise and counterclockwise channels are depicted in **Figure 21**a,b. The bidirectional MLFL always exists in pairs and

the soliton explosion dynamics occurs almost simultaneously in both channels. Temporal shift was observed during the soliton explosion process.[137,141] The temporal separation of the bidirectional MLFL was kept almost constant within 1 ns even though the energy was dramatically changed during the evolution process. In addition, similar spectral evolution was observed for the breathing soliton dynamics of the MLFL in both directions from background noise as shown in Figure 21c. The broadening of spectrum was attributed to the dramatically increased soliton energy till Q-ML stage was achieved. Next, a sudden spectral collapse was observed during the soliton explosion at ≈900 roundtrips, where the periodic spectral evolution of the soliton breathing was disrupted by a broad and chaotic spectrum. After the spectral collapse, the Q-ML dynamics were recovered. Figure 21d shows the energy evolution of the bidirectional MLFLs for both channels. The energy dramatically increased and decreased during the build-up and explosion processes, respectively. The apparent energy oscillation shows the breathing behavior of the DS-MLFL, as enclosed depicted in the inset of Figure 21d.

In addition to mode-locked EDFL, the soliton explosion dynamics in a mode-locked YDFL integrated with a nonlinear amplifying loop mirror was investigated in the net normal dispersion regime.[137] The real-time shot-to-shot spectrum reveals the soliton explosion dynamics in the transition regime of the DS-MLFL was experimentally measured through the TS-DFT technique over 100 consecutive roundtrips as shown in **Figure 22**a.
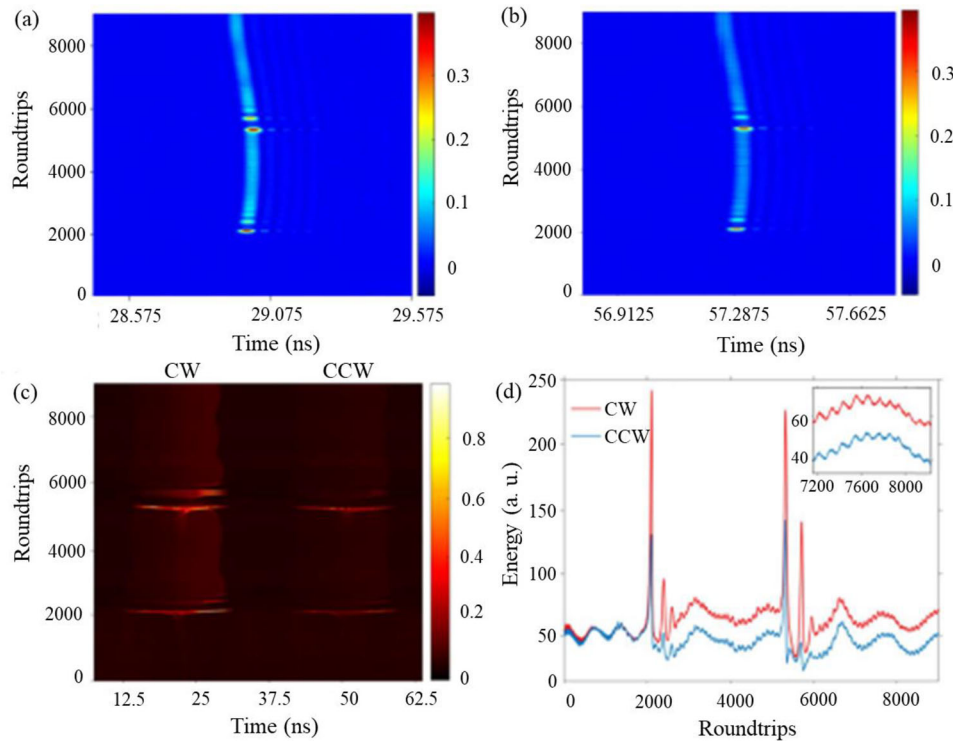
Figure 21. Real-time investigation of soliton explosion dynamics in the bidirectional MLFLs. Bidirectional SE-MLFLs propagate in the direction of a) clockwise and b) counterclockwise. Shot-to-shot measurement of c) spectral information and d) energy evolution. Reproduced with permission.[84] Copyright 2020, Chinese Laser Press.
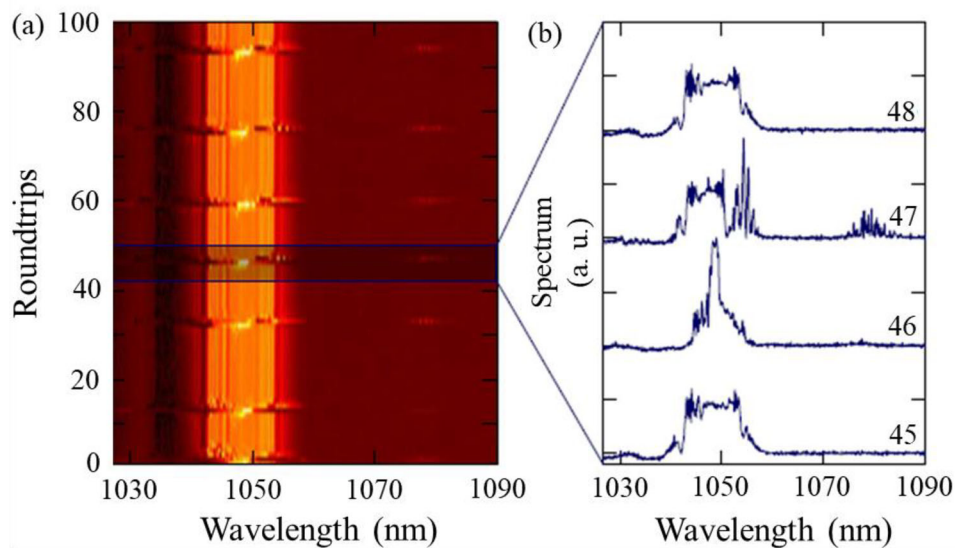

Figure 22. Real-time investigation of soliton explosion dynamics in a mode-locked EDFL. a) Shot-to-shot measurement over 100 roundtrips. b) Expanded view of a soliton explosion event from 45 to 48 roundtrips. Reproduced with permission.[137] Copyright 2015, Optica.

When the soliton explosion occurs, the DS-MLFL collapses into a narrower spectrum with a higher amplitude, which then reverts into the original state after a few roundtrips.[142] The four consecutive roundtrips from 45 to 48 around a particular soliton explosion event are depicted in Figure 22b. Apart from the collapse

and retrieval of the pulse at ≈1028 nm, the explosion event triggers the emission at ≈1075 nm for RTN at 47 roundtrips. Within 100 consecutive roundtrips, seven soliton explosion events were observed with qualitatively similar characteristics, intermittently without clear periodicity.
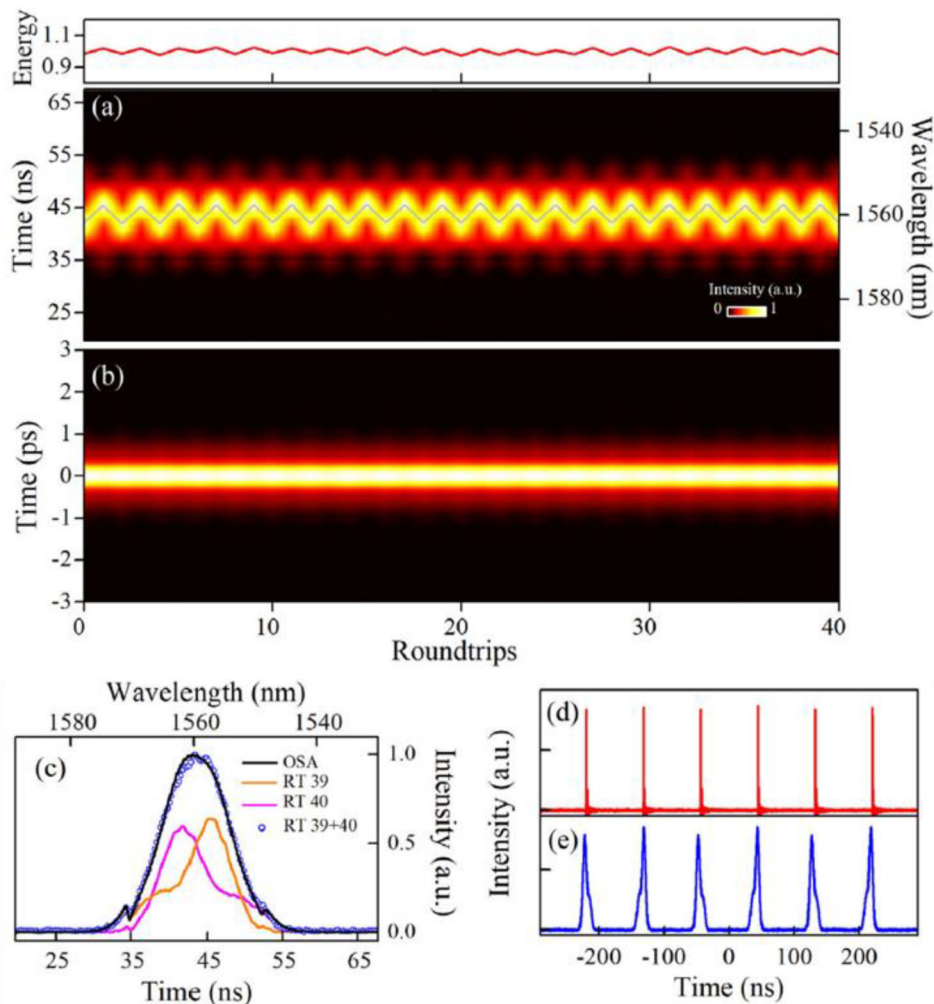
**ADVANCED
SCIENCE NEWS**

www.advancedsciencenews.com

www.lpr-journal.org

LASER
& PHOTONICS
REVIEWS

Figure 23. Real-time investigation of soliton trapping dynamics in a mode-locked EDFL. a) Real-time spectral information and time-stretched waveform. b) Field autocorrelation. c) Optical spectra. d,e) Shot-to-shot spectra at RT-39 and RT-40 with and without TS-DFT technique. Reproduced with permission.[145] Copyright 2021, Wiley-VCH GmbH & Co.

Apart from the mode-locked EDFL and YDFL, the motion dynamics of the soliton explosion in a mode-locked TDFL was experimentally observed in real-time through the TS-DFT technique.[143] The mode-locked TDFL has find growing interest for eye-safety applications due to the high absorption coefficient by the hydroxide (OH^-) groups at its working wavelengths. When pump power was adjusted to a transient pulsing state between single pulsing and double pulsing, a chaotic state was observed, which exhibits quasi-periodic evolution. This chaotic state shows several features, which includes period-doubling bifurcation, pulse splitting, soliton explosion, oscillatory behavior, and energy dissipation. This stationary soliton explosion occurs stochastically owing to the perturbation induced gain fluctuations. On the one hand, periodic soliton explosion was also observed due to soliton collision of dual-wavelength polarization multiplexed state. An extended recovery process was observed with multiperiodic modulation, i.e., polarization rotation effects and energy exchange between pulse polarization components with different birefringence characteristics.[107,144]

3.3.5. Soliton Trapping

The soliton trapping could be induced by the XPM in a nonlinear medium, where the birefringence and dispersion map could alter the wavelength of soliton, either blueshift or redshift periodically in an MLFL.[145] The XPM induces and sustains the vector asymmetrical soliton (VAS) with spectral period doubling, thus showing some interesting pulse trapping trajectories. The soliton trapping dynamics was studied in a MLFL integrated with an SWCNT-SA at a net GVD of ≈-0.05 ps².[145] **Figure 23**a presents the spectral and temporal information about the motion dynamics of the ST-MLFL over consecutive roundtrips. The zigzag pattern shows the oscillating peak wavelengths (λ_p) with a deviation of ≈4.3 nm, which looks like the evolution of SM vibration.[16,21] Figure 23b shows the corresponding field autocorrelation for the soliton trapping dynamics of the MLFL which is ≈1 ps over consecutive roundtrips. Figure 23c shows the shot-to-shot measurement at RT-39 and RT-40, which exhibit redshift and blueshift, respectively. Moreover, these roundtrips show asymmetrical profiles with different peak wavelengths and intensities.

Nevertheless, a nearly symmetrical Gaussian profile that matches the optical spectrum was generated in their superposition. The pulse trains measured with and without the TS-DFT technique are depicted in Figure 23d,e. For the pulse train measured with the TS-DFT technique, the two adjacent pulses show a clear intensity difference. On the other hand, smaller intensity modulation was generated for the laser output without the TS-DFT characterization. This fluctuation could be observed according to the energy (E) evolution as shown in the inset of Figure 23a, in which the integral of the spectral energy density $I(\omega)$ was calculated by

$$E = \Sigma\left[I(\omega) \cdot \Delta\omega\right] \tag{10}$$

where ω is the carrier frequency of photons and $\Delta\omega$ is the frequency interval. Furthermore, the optimization of intracavity polarization state could minimize the intensity modulation, which could hardly be distinguished from a stable mode-locking operation without the TS-DFT measurement. The experimental result was confirmed by numerical simulation based on the coupled Ginzburg–Landau equation (CGLE) to calculate the weak birefringent fibers.[145] The CGLE was solved with the standard symmetric split-step Fourier algorithm to obtain a stable solution. From numerical simulation, two polarization components exhibit slightly different evolution trajectories. The pulse was first compressed at each roundtrip and reached a minimum value at the position of the SA and then broadened into the following optical fiber. An obvious energy exchange was observed at the interval before the position of SA, denoting the pulse interaction. The SA induces optical loss thus the pulse energy drops abruptly for both odd-roundtrip numbers (i.e., RT-39) and even-roundtrip numbers (i.e., RT-40), which reflects the pulse interaction dynamics, or the so-called soliton trapping in the laser cavity.

The dynamical soliton trapping of polarization rotation vector soliton (PRVS) in a mode-locked EDFL integrated with a CNT-SA was investigated through the TS-DFT technique.[146] The PRVS exhibits the locking of soliton polarization rotation to a period equals the cavity roundtrip time or a multiple of this roundtrip time.[147] Moreover, PRVS shows the alteration of relative intensities of two polarization components between two or several values at the laser output, thus inducing dynamic soliton trapping. Besides pulse intensities, the two orthogonal polarization components in PRVS also exhibit periodical alteration in peak wavelengths and spectral profiles. Compared to soliton trapping in MLFL, PRVS shows dynamical soliton trapping where the peak wavelengths of two polarization components were shifted periodically to achieve soliton trapping at a fixed point of the mode-locked EDFL cavity.

3.3.6. Optical Rogue Wave

The optical rogue wave was first observed via extraordinary soliton-like pulses with extremely high intensity in supercontinuum generation.[148] An optical rogue wave is a transient wave occurring in a nonlinear system which exhibits three main characteristics, i.e., extremely large amplitude, long tail for pulse amplitude, and random evolution trajectories.[149] Before the demonstration of the TS-DFT technique, the optical rogue waves were studied merely by numerical simulation. For instance, the gener-

ation of dissipative rogue waves as a result of the inelastic collision and energy exchange of multiple pulses in a net anomalous dispersion MLFL was numerically studied through the NLSE.[150] In addition, the dissipative rogue waves in a net normal dispersion MLFL were also numerically studied.[151] Based on these numerical studies, the operation regimes of optical rogue waves are influenced by intracavity dispersion conditions. After the demonstration of the TS-DFT technique, the dynamics of optical rogue waves were revealed experimentally, which shows fascinating operation regimes in complex MLFL systems with distinct conditions, such as the net intracavity GVD,[151,152] mode-locking methods,[153–155] and laser cavity configurations.[156] For instance, an optical rogue wave was observed in the NLP regimes for both normal and anomalous GVD in an NPR-integrated mode-locked EDFL.[151] The intracavity GVD was controlled by changing the length of DCF. The real-time investigation of the motion dynamics in NLP-MLFL at net normal and anomalous GVD regimes was conducted through the TS-DFT technique over 1000 consecutive roundtrips as illustrated in **Figure 24**a,b. The spectral fluctuation of the anomalous GVD regime is more obvious than the normal GVD regime, which denotes the highly fluctuating temporal intensity distribution of the NLP at picosecond or sub-picosecond time scales. This observation matches the experimental result given by Runge et al.[157] Instead of investigating different GVD regimes, Runge et al.[157] compared the difference in the motion dynamics between soliton and NLP regimes in an NPR-integrated mode-locked EDFL where real-time measurement was conducted over 1000 consecutive roundtrips. The NLP-MLFL exhibits a higher pump power threshold than the S-MLFL, which could be achieved by properly adjusting the polarization state of the laser cavity. The spectra of the S-MLFL are nearly indistinguishable from each other over the entire roundtrip with Kelly's sidebands. On the other hand, substantial fluctuations were observed in NLP-MLFL over the entire roundtrip. In a normal dispersion NPR-integrated mode-locked YDFL with a net GVD of ≈0.09 ps^2, the waveplates and the orientation of the birefringence filter were adjusted to achieve noise burst in the DS-MLFL operation regime.[152] The real-time measurement was conducted over 1000 consecutive roundtrips. For the stable DS-MLFL regime, the spectra are indistinguishable and exhibit sharp peaks at the edges with typical rectangular spectral profile,[158] which agrees with the observation by Luo et al.[159] By contrast, rigorous fluctuations were observed for NLP-MLFL based on the real-time shot-to-shot measurement.

Besides the NPR method, a nonlinear amplifying loop mirror was also employed to generate optical rogue waves.[156] The shot-to-shot spectral fluctuations of a Raman-destabilized NLP operating in a mode-locked YDFL was observed with its sporadic emission of Raman pulses over 350 consecutive roundtrips. The Raman emission at ≈1075 nm increased dramatically when the pump power was increased from 190 to 230 mW. Strong fluctuations with high pulse amplitude were clearly resolved by Raman emission both at ≈1028 and ≈1075 nm, implying the formation of an NLP-induced Raman rogue wave. Apart from artificial SAs, SESAM,[154] CNT-SA,[153] and graphene–SA[155] were integrated to generate optical rogue waves in the mode-locked EDFLs. The dissipative rogue wave was generated due to single-soliton collision that disrupt the stable mode-locking operation by increasing the pump power.[153] During soliton explosion, a random and
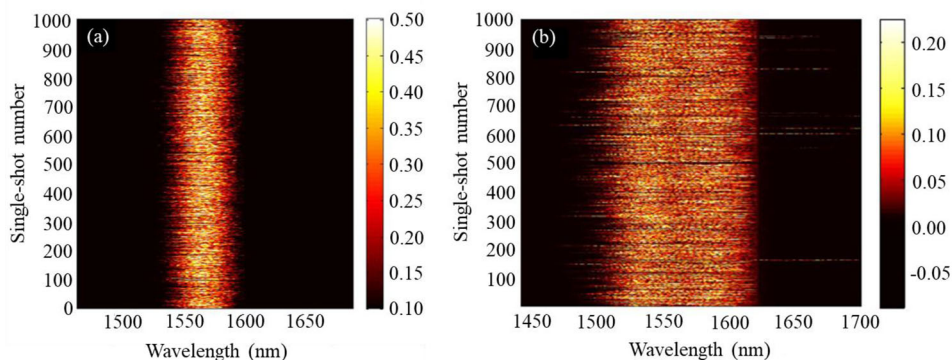
ADVANCED
SCIENCE NEWS

www.advancedsciencenews.com

LASER
& PHOTONICS
REVIEWS

www.lpr-journal.org

Figure 24. Real-time investigation of optical rogue wave dynamics operating in the NLP regimes. The NLP-MLFL operating at the a) normal and b) anomalous GVD regimes. Reproduced with permission.[151] Copyright 2014, American Physical Society.

abrupt increase in nanosecond pulse amplitude was observed within 700 consecutive roundtrips. High amplitude waves were unpredictably generated as a transient state, which was disappeared in a soliton explosion event across six roundtrips. Apart from single-soliton explosion, the investigation of dissipative rogue waves was also conducted on multisoliton explosion by using higher pump power and adjusting the polarization states.[154] Besides, the optical rogue waves with high nanosecond pulse amplitude were generated from an NLP-MLFL with multiple wave packets.[155] These wave packets were generated due to nonlinear interaction and soliton collision that exhibit pulse breaking and shaping of localized mode-locked NLP pulses.

Based on the above studies, the NLP-MLFL is frequently used to observe the optical rogue waves. The NLP-MLFL was shifted from DS-MLFL by rotating the polarization beam splitter (PBS) with a tilt angle from $-5°$ to $+5°$, which modulates the instantaneous power of the laser pulse in an NPR-integrated mode-locked YDFL.[53] The modulation of instantaneous power contributes to the pulse operation in different saturable absorption regions.[160] Apart from the PBS angles, the DS-MLFL and NLP-MLFL were achieved at different pump power thresholds of 380 and 290 mW, respectively. The pulse evolution dynamics for the DS-MLFL experience five stages, i.e., Q-switching, raised and damped relaxation oscillation, noise-like, successive soliton explosions, and finally soliton breathing stages. On the other hand, the NLP-MLFL experiences only two stages, which are raised RO and Q-switching stages. The NLP-MLFL exhibits a higher pulse energy than DS-MLFL thus showing a shorter build-up time during the raised RO stage. There are several factors affecting the final state of stable DS-MLFL or NLP-MLFL, i.e., the single or multiple pulses output, roundtrip loss, and the magnitude of nonlinearity of the MLFLs. A switching behavior from the DS-MLFL to loosely bound solitons and NLP-MLFL was observed by increasing the pump power and adjusting intracavity polarization state.[161] Apart from mode-locked YDFL, the investigation of stable DS-MLFL and NLP-MLFL regimes was also studied in an NPR-integrated mode-locked TDFL, where the switching between these operation regimes was also realized by adjusting the pump power and polarization states.[112] Moreover, the real-time investigation of build-up and evolution dynamics in the NLP-MLFL was also studied in an NPR-integrated mode-locked EDFL in both the net normal and anomalous

dispersion regimes.[162] The major differences between these dispersion regimes observed during the initial stages have been unraveled experimentally. For instance, the interplay between gain, SPM, and dispersion contributes to the larger fluctuations in the dynamics of initial stage at the net normal dispersion regime. On the contrary, soliton pulse shaping dominates the evolution process in the net anomalous dispersion regime, which maintains the pulse integrity over a longer time.

4. Challenges and Recommendations

The real-time investigation of the MLFL dynamics has encountered several challenges. First and foremost, the buildup processes of DS and soliton are both sensitive to external perturbations, i.e., polarization state modification and pump power fluctuation.[7,31] The fluctuation during the buildup process for these MLFLs becomes more rigorous when the laser cavities were integrated with the NPR method. The combination of the NPR method and material-based SA such as SWCNT could solve this issue by suppressing the Q-switched lasing, as shown in **Figure 25**a.[7] Several hundreds of optical pulses were contained in each Q-switched pulse as indicated in the inset of Figure 25a. Moreover, Figure 25b shows that a longer nascent time of ≈ 80 ms with 76 lines of Q-switched lasing was attained when only the NPR method was integrated into MLFL. By increasing the pump power, the Q-switched lasing with an even longer nascent time of ≈ 160 ms was obtained as shown in Figure 25c. It has been generally accepted that Q-switched lasing is the source of instabilities prior to the formation of the single-pulse MLFL. Therefore, the implementation of a material-based SA could improve the build-up process for stable mode-locking. Apart from SWCNT-SA, other materials such as graphene,[163] perovskite,[164] and MXene[165] could also be investigated due to their different nonlinearity parameters, i.e., modulation depths and nonsaturable losses that may lead to the differences in the buildup process of stable MLFL.

The real-time investigation of MLFL dynamics is dependent on the appropriate pump power and precise polarization state, as reported for SM-MLFL,[21,31,97] S-MLFL,[7] DS-MLFL and NLP-MLFL,[53,112,161] bidirectional soliton,[89] breathing DS,[18] soliton trapping,[145,146] and optical rogue wave for soliton and NLP dynamics.[157] In these nonpolarization-maintaining laser setups,
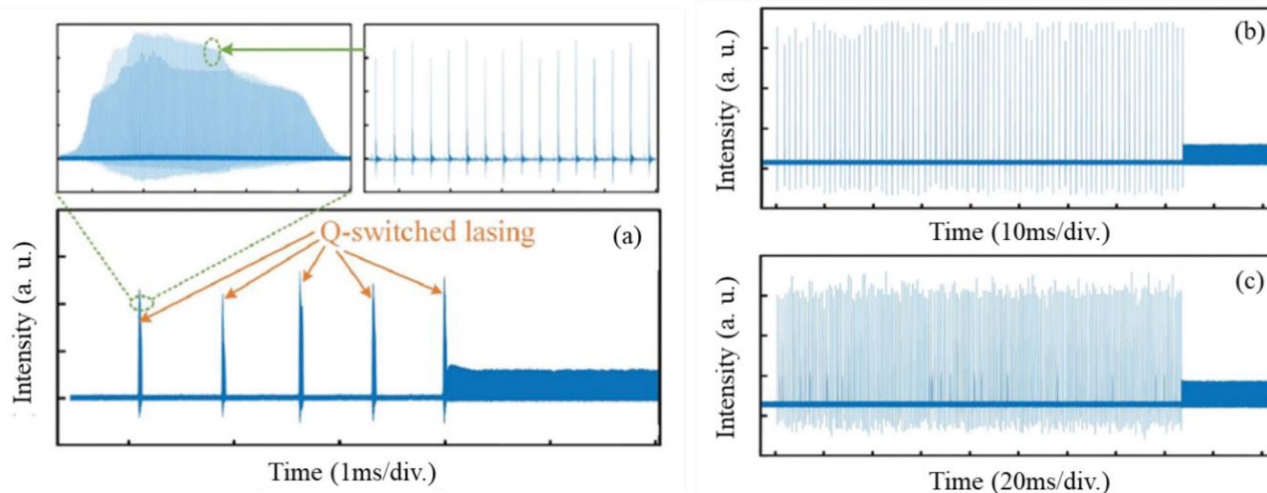
**ADVANCED
SCIENCE NEWS**

www.advancedsciencenews.com

LASER &
PHOTONICS
REVIEWS

www.lpr-journal.org

Figure 25. Build-up and evolution process in the MLFL experiencing Q-switched lasing stage. The SAs integrated with a) the combination of the NPR method and an SWCNT-SA, and only the NPR method with b) weaker and c) stronger pump powers. Reproduced with permission.[7] Copyright 2019, Chinese Laser Press.

a precise polarization state is important to achieve the desired dynamics. However, the polarization states were merely adjusted without emphasizing the polarization angles or exact polarization states.[19,87,166] The unknown polarization information hinders further investigation on the polarization state at the interval prior to formation of desired dynamics, i.e., precise polarization angle variation of 1° or less. Therefore, real-time investigation on precise polarization angle variation for the MLFL dynamics is recommended, for instance, by using a polarimeter system together with PBS or polarization controller with displayed angles.[167]

In most previous studies, the real-time investigation into the MLFL dynamics was performed on the EDFL. This is due to the simpler, cheaper, and suitable dispersive optical fibers, i.e., DCF or SMF-28e at ≈1.55 μm. Occasionally, the TS-DFT technique has been employed for the investigation of mode-locked YDFLs[28,53–55,66,137,152] and TDFLs.[112,143] The TS-DFT technique has rarely been incorporated for mode-locked lasers operating in the visible region and at the wavelength of ≈2.0 μm or above. For the TS-DFT detection system at ≈1.06 μm, SMF-28e was employed as the dispersive medium. To compare with the SMF-28e, Hi1060 optical fiber could be tested in the TS-DFT detection system due to its efficient fiber coupling and dispersion of ≈−38 ps (nm km)$^{-1}$ for Corning HI 1060 optical fiber at ≈1.06 μm. In the NIR region between operation wavelengths of YDFL and EDFL (≈1.06 to 1.55 μm) and between EDFL and TDFL (≈1.55 to 1.75 μm), mode-locked bismuth-doped fiber laser (BDFL) was demonstrated, whilst most articles were reported by Dianov and co-workers.[168,169] In particular, the mode-locked BDFL at ≈1.3 μm is attractive because the second telecommunication window has low loss and weak chromatic dispersion for silica fiber.[170–172] Therefore, the real-time investigation of dynamics, i.e., the birth, evolution and extinction trajectories, complex stationary, and motion dynamics in mode-locked BDFL is recommended. Besides that, the real-time investigation of soliton molecule and soliton explosion was conducted for the mode-locked TDFLs due to the acceptable loss of SMF-28e at ≈1.7 μm.[112,143] Recently, the TS-DFT technique was also em-

ployed for the investigation of pulse instability and transient dynamics in mid-infrared MLFL, with focus on the quasi-stable pulsation, pulse-collapse and buildup of soliton-pair.[173] A challenge of investigating the real-time dynamics at the wavelength of ≈2 μm or above such as mid-infrared MLFL is the lacking of dispersive medium to stretch the spectral profile into time-stretched waveform. Therefore, it is important to explore a suitable dispersive medium to the TS-DFT technique integrated at the wavelength of ≈2 μm or above. Apart from that, visible MLFL is a rather new topic and was reported recently for red lasers operating at ≈635 nm and investigation of the real-time dynamics could be interesting.[174–176] In addition, more MLFL at visible range can be explored in near future. For instance, a 3.6 W continuous wave praseodymium-doped green laser at ≈521 nm was demonstrated and supposed to achieve mode-locking operation.[177] However, a challenge in stretching the spectral profile of visible MLFL is the high loss of dispersive media, i.e., SMF-28e, DCF, and Hi1060 optical fiber in the visible region, which should be solved before the TS-DFT techniques can be executed. In contrast to the real-time investigation in near-infrared region, the TS-DFT technique has been seldom employed for the study of dynamics in both visible and mid-infrared regions. Therefore, it is very interesting if the TS-DFT technique could be employed to study the MLFL in the visible and at ≈2 μm or above in future.

Apart from the TS-DFT technique, the transformation from real-time spectral information to temporal information can be observed and investigated using time lens technique. The time lens is a temporal magnifier technique, which reveals the single-shot temporal information, i.e., pulse profile and pulse width,[50] based on space-time duality (STD) theory.[178] The STD is integrated from the equivalence of electromagnetic beam diffraction and dispersive pulse propagation that contribute to a quadratic phase modulation in time.[179] The time lens system exhibits an asynchronous FWM temporal magnifier regime, which shows relatively simpler and longer recording length than synchronous systems like those utilized for the investigation of the dynamics in optical rogue waves in integrable turbulence[180] and

spontaneous breather events in optical modulation instability.[181] For instance, the dynamics of soliton pairs,[179] soliton creeping,[182] and collision dissipative SM[183] were investigated in a net anomalous mode-locked EDFL, whereas DS dynamics were characterized in a net normal mode-locked EDFL,[50] using both TS-DFT technique and asynchronous time lens system. The time lens technique was also employed to investigate the multiscale laser dynamics,[30] optical rogue wave structures in the NLP,[184] and optical rogue wave patterns in the MLFL with single-peak, twin-peaks, and triple-peaks time scales.[185] Apart from understanding the dynamics in both spectral and temporal domain, several factors should be considered during the real-time investigation, i.e., phase, polarization, and space evolution dynamics. For instance, the evolution dynamics of phase and polarization were solved for buildup of dissipative soliton molecules,[97] optical trapping,[145] harmonic mode-locking,[72] soliton breather,[186] and breather molecular complexes,[113] whereas the space evolution dynamics were studied in spatiotemporal solitons.[187] Therefore, apart from the TS-DFT technique, the integration of time lens system and the evolution dynamics in terms of phase, polarization, and space is recommended to enable a more comprehensive investigation of real-time dynamics in MLFL.

5. Conclusion and Outlook

We have discussed the recent progress on the investigation of MLFL dynamics through the TS-DFT technique. The TS-DFT technique provides linear dispersion of localized MLFL pulses in a dispersive medium which maps the spectral information of an ultrashort optical pulse into a time-stretched waveform. This makes the real-time investigations of ultrafast dynamics in MLFL a reality. These real-time investigations enable the probe of the dynamics of birth, evolution, and extinction process in MLFL working at different dispersion regimes, which consist of soliton, dissipative soliton, stretched pulse, and soliton similariton. Moreover, different types of MLFL and complex motion dynamics in MLFL were studied through the TS-DFT technique. The different types of MLFL include HML and bidirectional MLFL, whereas the complex motion dynamics in MLFL consists of soliton molecules, soliton breathing, soliton bifurcation, soliton explosion, soliton trapping, and optical rogue waves. Apart from the various dynamics process and phenomena studied through the TS-DFT technique, the current issues and challenges met by the TS-DFT technique were also discussed. Several recommendations were provided to enable a more comprehensive investigation of real-time dynamics in MLFL through the TS-DFT technique. This review is expected to provide a deeper insight into the MLFL dynamics, and the use of the TS-DFT technique is expected to unveil plenty of fascinating MLFL dynamics and unexplored trajectories that could be of growing interest among the laser community.

Conflict of Interest

The authors declare no conflict of interest.

[1] T. Udem, R. Holzwarth, T. W. Hänsch, *Nature* **2002**, *416*, 233.
[2] T. Steinmetz, T. Wilken, C. Araujo-Hauck, R. Holzwarth, T. W. Hänsch, L. Pasquini, A. Manescau, S. D'Odorico, M. T. Murphy, T. Kentischer, W. Schmidt, T. Udem, *Science* **2008**, *321*, 1335.
[3] C. Kerse, H. Kalaycıoğlu, P. Elahi, B. Çetin, D. K. Kesim, Ö. Akçaalan, S. Yavaş, M. D. Aşık, B. Öktem, H. Hoogland, R. Holzwarth, F. Ö. Ilday, *Nature* **2016**, *537*, 84.
[4] D. Strickland, G. Mourou, *Opt. Commun.* **1985**, *56*, 219.
[5] M. Fridman, M. Nixon, E. Ronen, A. A. Friesem, N. Davidson, *Opt. Lett.* **2010**, *35*, 526.
[6] X. Yi, Q. F. Yang, K. Y. Yang, K. Vahala, *Nat. Commun.* **2018**, *9*, 3565.
[7] X. Liu, Y. Cui, *Adv. Photonics* **2019**, *1*, 016003.
[8] N. Seymour-Smith, P. Blythe, M. Keller, W. Lange, *Rev. Sci. Instrum.* **2010**, *81*, 075109.
[9] S. Yun, G. Tearney, B. Bouma, B. Park, J. de Boer, *Opt. Express* **2003**, *11*, 3598.
[10] A. C. Scott, F. Y. F. Chu, D. W. Mclaughlin, *Proc. IEEE* **1973**, *61*, 1443.
[11] N. Jiménez, A. Mehrem, R. Picó, L. M. García-Raffi, V. J. Sánchez-Morcillo, *C. R. Phys.* **2016**, *17*, 543.
[12] H. A. Haus, W. S. Wong, *Rev. Mod. Phys.* **1996**, *68*, 423.
[13] A. Hasegawa, *Chaos* **2000**, *10*, 475.
[14] M. Bilal, S.-U. Rehman, J. Ahmad, *J. Ocean Eng. Sci.* **2022**, https://doi.org/10.1016/j.joes.2022.05.027.
[15] N. N. Akhmediev, A. Ankiewicz, J. M. Soto-Crespo, *J. Opt. Soc. Am. B* **1998**, *15*, 515.
[16] G. Herink, F. Kurtz, B. Jalali, D. R. Solli, C. Ropers, *Science* **2017**, *356*, 50.
[17] D. R. Solli, G. Herink, B. Jalali, C. Ropers, *Nat. Photonics* **2012**, *6*, 463.
[18] J. Peng, S. Boscolo, Z. Zhao, H. Zeng, *Sci. Adv.* **2019**, *5*, 1.
[19] K. Zhao, X. Xiao, C. Yang, *Photonics Res.* **2021**, *9*, 289.
[20] S. Chouli, P. Grelu, *Phys. Rev. A* **2010**, *81*, 063829.
[21] R. Xia, Y. Luo, P. P. Shum, W. Ni, Y. Liu, H. Q. Lam, Q. Sun, X. Tang, L. Zhao, *Opt. Lett.* **2020**, *45*, 1551.
[22] Y. Wang, C. Wang, F. Zhang, J. Guo, C. Ma, W. Huang, Y. Song, Y. Ge, J. Liu, H. Zhang, *Rep. Prog. Phys.* **2020**, *83*, 116401.
[23] L. Huang, Y. Zhang, X. Liu, *Nanophotonics* **2020**, *9*, 2731.
[24] A. Mahjoubfar, D. V. Churkin, S. Barland, N. Broderick, S. K. Turitsyn, B. Jalali, *Nat. Photonics* **2017**, *11*, 341.
[25] K. Goda, B. Jalali, *Nat. Photonics* **2013**, *7*, 102.

[26] C. Lei, B. Guo, Z. Cheng, K. Goda, *Appl. Phys. Rev.* **2016**, *3*, 011102.

[27] T. Godin, L. Sader, A. K. Kashi, P.-H. Hanzard, A. Hideur, D. J. Moss, R. Morandotti, G. Genty, J. M. Dudley, A. Pasquazi, M. Kues, B. Wetzel, *Adv. Phys. X* **2022**, *7*, 2067487.

[28] M. Suzuki, O. Boyraz, H. Asghari, B. Jalali, *Sci. Rep.* **2020**, *10*, 14460.

[29] K. Goda, D. R. Solli, K. K. Tsia, B. Jalali, *Phys. Rev. A* **2009**, *80*, 043821.

[30] X. Wei, B. Li, Y. Yu, C. Zhang, K. K. Tsia, K. K. Y. Wong, *Opt. Express* **2017**, *25*, 29098.

[31] X. Liu, X. Yao, Y. Cui, *Phys. Rev. Lett.* **2018**, *121*, 023905.

[32] H. Liang, X. Zhao, B. Liu, J. Yu, Y. Liu, R. He, J. He, H. Li, Z. Wang, *Nanophotonics* **2020**, *9*, 1921.

[33] G. Herink, B. Jalali, C. Ropers, D. R. Solli, *Nat. Photonics* **2016**, *10*, 321.

[34] J. Azaña, M. A. Muriel, *IEEE J. Quantum Electron.* **2000**, *36*, 517.

[35] E. D. Diebold, N. K. Hon, Z. Tan, J. Chou, T. Sienicki, C. Wang, B. Jalali, *Opt. Express* **2011**, *19*, 23809.

[36] S. Yegnanarayanan, P. D. Trinh, B. Jalali, *Opt. Lett.* **1996**, *21*, 740.

[37] S. Liu, Y. Chen, L. Huang, T. Cao, X. Qin, H. Ning, J. Yan, K. Hu, Z. Guo, J. Peng, *Opt. Lett.* **2021**, *46*, 2376.

[38] M. Hoshikawa, K. Ishii, T. Makino, T. Hashimoto, H. Furukawa, N. Wada, *Opt. Rev.* **2020**, *27*, 246.

[39] J. Peng, M. Sorokina, S. Sugavanam, N. Tarasov, D. V. Churkin, S. K. Turitsyn, H. Zeng, *Commun. Phys.* **2018**, *1*, 1.

[40] A. Bednyakova, S. K. Turitsyn, *Phys. Rev. Lett.* **2015**, *114*, 113901.

[41] H. J. Chen, M. Liu, J. Yao, S. Hu, J. B. He, A. P. Luo, Z. C. Luo, W. C. Xu, *IEEE Photonics J.* **2018**, *10*, 1501809.

[42] K. Krupa, K. Nithyanandan, U. Andral, P. Tchofo-Dinda, P. Grelu, *Phys. Rev. Lett.* **2017**, *118*, 243901.

[43] X. Liu, D. Popa, N. Akhmediev, *Phys. Rev. Lett.* **2019**, *123*, 093901.

[44] Y. Cui, X. Liu, *Photonics Res.* **2019**, *7*, 423.

[45] Y. S. Cui, Z. K. Dong, L. L. Zhang, J. R. Tian, Y. R. Song, *Laser Phys. Lett.* **2021**, *18*, 085104.

[46] A. Chong, W. H. Renninger, F. W. Wise, *Opt. Lett.* **2007**, *32*, 2408.

[47] S. K. Turitsyn, B. G. Bale, M. P. Fedoruk, *Phys. Rep.* **2012**, *521*, 135.

[48] V. V. Afanasjev, N. Akhmediev, *Phys. Rev. E* **1996**, *53*, 6471.

[49] H. J. Chen, M. Liu, J. Yao, S. Hu, J. B. He, A. P. Luo, W. C. Xu, Z. C. Luo, *Opt. Express* **2018**, *26*, 2972.

[50] P. Ryczkowski, M. Närhi, C. Billet, J. M. Merolla, G. Genty, J. M. Dudley, *Nat. Photonics* **2018**, *12*, 221.

[51] Y. Cao, L. Gao, S. Wabnitz, H. Ran, L. Kong, T. Zhu, *Opt. Laser Technol.* **2021**, *133*, 106512.

[52] D. Y. Tang, L. M. Zhao, B. Zhao, A. Q. Liu, *Phys. Rev. A* **2005**, *72*, 043816.

[53] Z. Zhang, J. Tian, Y. Cui, Y. Wu, Y. Song, *Chin. Opt. Lett.* **2022**, *20*, 081402.

[54] H. Zhao, G. M. Ma, X. Y. Li, T. J. Li, H. Cui, M. Liu, A. P. Luo, Z. C. Luo, W. C. Xu, *Opt. Express* **2020**, *28*, 24550.

[55] D. Mao, Z. He, Y. Zhang, Y. Du, C. Zeng, L. Yun, Z. Luo, T. Li, Z. Sun, J. Zhao, *Light: Sci. Appl.* **2022**, *11*, 1.

[56] K. Tamura, E. P. Ippen, H. A. Haus, L. E. Nelson, *Opt. Lett.* **1993**, *18*, 1080.

[57] F. Ö. Ilday, J. R. Buckley, H. Lim, F. W. Wise, W. G. Clark, *Opt. Lett.* **2003**, *28*, 1365.

[58] H. A. Haus, K. Tamura, L. E. Nelson, E. P. Ippen, *IEEE J. Quantum Electron.* **1995**, *31*, 591.

[59] D. Han, Z. Hui, J. Xie, K. Ren, J. Gong, F. Zhao, J. Dong, D. Li, X. Xin, *Infrared Phys. Technol.* **2019**, *102*, 102984.

[60] F. W. Wise, A. Chong, W. H. Renninger, *Laser Photonics Rev.* **2008**, *2*, 58.

[61] X. Wang, X. Ren, J. Peng, X. Shen, K. Huang, Y. Yan, H. Zeng, *Opt. Express* **2019**, *27*, 2732.

[62] B. Oktem, C. Ülgüdür, F. Ö. Ilday, *Nat. Photonics* **2010**, *4*, 307.

[63] C. Lapre, C. Billet, F. Meng, P. Ryczkowski, T. Sylvestre, C. Finot, G. Genty, J. M. Dudley, *Sci. Rep.* **2019**, *9*, 13950.

[64] J. M. Dudley, *Nat. Photonics* **2010**, *4*, 272.

[65] F. Meng, C. Lapre, C. Billet, G. Genty, J. M. Dudley, *Opt. Lett.* **2020**, *45*, 1232.

[66] C. Ma, G. Wu, B. Gao, Y. Wang, J. Liu, H. Zhang, *Opt. Laser Technol.* **2022**, *156*, 108486.

[67] Y. Wang, J. Li, K. Mo, Y. Wang, L. Fei, Y. Liu, *Sci. Rep.* **2017**, *7*, 7779.

[68] J. Li, C. Wang, P. Wang, *J. Light. Technol.* **2022**, *40*, 5958.

[69] V. A. Ribenek, D. A. Stoliarov, D. A. Korobko, A. A. Fotiadi, *Opt. Lett.* **2021**, *46*, 5687.

[70] J. N. Kurtz, *SIAM Rev.* **2006**, *48*, 629.

[71] A. B. Grudinin, S. Gray, *J. Opt. Soc. Am. B* **1997**, *14*, 144.

[72] X. Liu, M. Pang, *Laser Photonics Rev.* **2019**, *13*, 1800333.

[73] A. B. Grudinin, W. H. Loh, V. V. Afanasjev, D. N. Payne, *Opt. Lett.* **1994**, *19*, 698.

[74] J. M. Soto-Crespo, N. Akhmediev, P. Grelu, F. Belhache, *Opt. Lett.* **2003**, *28*, 1757.

[75] D. A. Korobko, O. G. Okhotnikov, I. O. Zolotovskii, *Opt. Lett.* **2015**, *40*, 2862.

[76] R. Weill, A. Bekker, V. Smulakovsky, B. Fischer, O. Gat, *Optica* **2016**, *3*, 189.

[77] S. Gray, A. B. Grudinin, W. H. Loh, D. N. Payne, *Opt. Lett.* **1995**, *20*, 189.

[78] X. Wang, J. Peng, K. Huang, M. Yan, H. Zeng, *Opt. Express* **2019**, *27*, 28808.

[79] J. Zeng, M. Y. Sander, *Opt. Lett.* **2020**, *45*, 5.

[80] T. Ideguchi, T. Nakamura, Y. Kobayashi, K. Goda, *Optica* **2016**, *3*, 748.

[81] Q. F. Yang, X. Yi, K. Y. Yang, K. Vahala, *Nat. Photonics* **2017**, *11*, 560.

[82] S. Mehravar, R. A. Norwood, N. Peyghambarian, K. Kieu, *Appl. Phys. Lett.* **2016**, *108*, 231104.

[83] J. M. Jiang, X. J. Chen, Y. X. Gao, M. Liu, Z. A. Bai, A. P. Luo, W. C. Xu, Z. C. Luo, *Opt. Laser Technol.* **2021**, *142*, 107196.

[84] Y. Zhou, Y.-X. Ren, J. Shi, K. K. Y. Wong, *Photonics Res.* **2020**, *8*, 1566.

[85] Y. Yu, C. Kong, B. Li, J. Kang, Y. X. Ren, Z. C. Luo, K. K. Y. Wong, *Opt. Lett.* **2019**, *44*, 4813.

[86] I. Kudelin, S. Sugavanam, M. Chernysheva, *Photonics Res.* **2020**, *8*, 776.

[87] K. Yang, T. J. Li, X. D. Li, J. X. Chen, M. Liu, H. Cui, A. P. Luo, W. C. Xu, Z. C. Luo, *Opt. Lett.* **2021**, *46*, 2021.

[88] C. Zeng, X. Liu, L. Yun, *Opt. Express* **2013**, *21*, 18937.

[89] C. Wang, Y. Li, D. Huang, H. Chen, Y. Shi, F. Li, *Phys. Rev. A* **2022**, *105*, 043515.

[90] J. He, P. Wang, R. He, C. Liu, M. Zhou, Y. Liu, Y. Yue, B. Liu, D. Xing, K. Zhu, K. Chang, Z. Wang, *Opt. Express* **2022**, *30*, 14218.

[91] Y. Zhou, Y.-X. Ren, J. Shi, K. K. Y. Wong, *Adv. Photonics Res.* **2022**, *3*, 2100318.

[92] Y. Zhou, Y.-X. Ren, J. Shi, K. K. Y. Wong, *Opt. Lett.* **2022**, *47*, 1968.

[93] G. I. Stegeman, M. Segev, *Science* **1999**, *286*, 1518.

[94] M. Stratmann, T. Pagel, F. Mitschke, *Phys. Rev. Lett.* **2005**, *95*, 1.

[95] W. Wang, L. Wang, W. Zhang, *Adv. Photonics* **2020**, *2*, 034001.

[96] Z. Q. Wang, K. Nithyanandan, A. Coillet, P. Tchofo-Dinda, P. Grelu, *Nat. Commun.* **2019**, *10*, 830.

[97] J. Peng, H. Zeng, *Laser Photonics Rev* **2018**, *12*, 1800009.

[98] J. G. Rarity, J. Fluconis, J. Duligall, W. J. Wadsworth, P. S. J. Russell, *Opt. Express* **2005**, *13*, 534.

[99] A. Komarov, K. Komarov, F. Sanchez, *Phys. Rev. A* **2009**, *79*, 033807.

[100] B. A. Malomed, *Phys. Rev. A* **1991**, *44*, 6954.

[101] Y. Wang, F. Leo, J. Fatome, M. Erkintalo, S. G. Murdoch, S. Coen, *Optica* **2017**, *4*, 855.

[102] M. Liu, H. Li, A. P. Luo, H. Cui, W. C. Xu, Z. C. Luo, *J. Opt.* **2018**, *20*, 034010.

[103] Y. Zhou, Y.-X. Ren, J. Shi, H. Mao, K. K. Y. Wong, *Optica* **2020**, *7*, 965.

[104] Y. Zhang, C. Zhao, X. Wu, Y. Meng, J. Ge, *IEEE Photonics Technol. Lett.* **2022**, *34*, 583.

[105] J. Peng, H. Zeng, *Opt. Lett.* **2019**, *44*, 2899.

[106] J. Li, H. Li, Z. Wang, Z. Zhang, S. Zhang, Y. Liu, *Photonics* **2022**, *9*, 489.

[107] C. Anastassiou, M. Segev, K. Steiglitz, J. A. Giordmaine, M. Mitchell, M. F. Shih, S. Lan, J. Martin, *Phys. Rev. Lett.* **1999**, *82*, 2332.

[108] S. Stalin, R. Ramakrishnan, M. Senthilvelan, M. Lakshmanan, *Phys. Rev. Lett.* **2019**, *122*, 043901.

[109] Y. Zhou, Y.-X. Ren, J. Shi, K. K. Y. Wong, *Opt. Express* **2022**, *30*, 21931.

[110] Y. Wei, B. Li, X. Wei, Y. Yu, K. K. Y. Wong, *Appl. Phys. Lett.* **2018**, *112*, 081104.

[111] J. M. Soto-Crespo, P. Grelu, N. Akhmediev, N. Devine, *Phys. Rev. E* **2007**, *75*, 016613.

[112] J. X. Chen, X. Y. Li, T. J. Li, Z. Y. Zhan, M. Liu, C. Li, A. P. Luo, P. Zhou, K. K. Y. Wong, W. C. Xu, Z. C. Luo, *Photonics Res.* **2021**, *9*, 873.

[113] J. Peng, Z. Zhao, S. Boscolo, C. Finot, S. Sugavanam, D. V. Churkin, H. Zeng, *Laser Photonics Rev.* **2021**, *15*, 2000132.

[114] Y. Luo, Y. Xiang, P. P. Shum, Y. Liu, R. Xia, W. Ni, H. Q. Lam, Q. Sun, X. Tang, *Opt. Express* **2020**, *28*, 4216.

[115] H. J. Chen, Y. J. Tan, J. G. Long, W. C. Chen, W. Y. Hong, H. Cui, A. P. Luo, Z. C. Luo, W. C. Xu, *Opt. Express* **2019**, *27*, 28507.

[116] C. Lecaplain, P. Grelu, C. Conti, *Opt. Lett.* **2014**, *39*, 263.

[117] J. Peng, H. Zeng, *Phys. Rev. Appl.* **2019**, *12*, 034052.

[118] C. Lapre, C. Billet, F. Meng, G. Genty, J. M. Dudley, *OSA Continuum* **2020**, *3*, 275.

[119] Q. Huang, Z. Huang, Z. Luo, C. Mou, *Opt. Lett.* **2021**, *46*, 5683.

[120] L. Q. English, M. Sato, A. J. Sievers, *Phys. Rev. B* **2003**, *67*, 024403.

[121] Z. W. Wei, M. Liu, S. X. Ming, A. P. Luo, W. C. Xu, Z. C. Luo, *Opt. Lett.* **2018**, *43*, 5965.

[122] Y. Luo, R. Xia, P. P. Shum, W. Ni, Y. Liu, H. Q. Lam, Q. Sun, X. Tang, L. Zhao, *Photonics Res.* **2020**, *8*, 884.

[123] F. O. Ilday, F. W. Wise, *Opt. Lett.* **2002**, *27*, 1531.

[124] Y. Du, M. Han, P. Cheng, X. Shu, *Opt. Lett.* **2019**, *44*, 4087.

[125] D. Turaev, A. G. Vladimirov, S. Zelik, *Phys. Rev. Lett.* **2012**, *108*, 263906.

[126] A. Komarov, F. Amrani, A. Dmitriev, K. Komarov, D. Meshcheriakov, F. Sanchez, *Phys. Rev. A* **2012**, *85*, 013802.

[127] Z. X. Zhang, M. Luo, J. X. Chen, L. H. Chen, M. Liu, A. P. Luo, W. C. Xu, Z. C. Luo, *Opt. Lett.* **2022**, *47*, 1750.

[128] X. Wu, Y. Zhang, J. Song, S. Boscolo, C. Finot, H. Zeng, *Nat. Commun.* **2022**, *13*, 5784.

[129] J. M. Soto-Crespo, N. Akhmediev, A. Ankiewicz, *Laser Photonics Rev.* **2000**, *85*, 2937.

[130] E. N. Tsoy, N. Akhmediev, *Phys. Lett. A* **2005**, *343*, 417.

[131] E. N. Tsoy, A. Ankiewicz, N. Akhmediev, *Phys. Rev. E* **2006**, *73*, 36621.

[132] J. M. Soto-Crespo, M. Grapinet, P. Grelu, N. Akhmediev, *Phys. Rev. E* **2004**, *70*, 66612.

[133] K. Krupa, T. M. Kardaś, Y. Stepanenko, *Laser Photonics Rev.* **2022**, *16*, 2100646.

[134] M. Liu, Z. Wei, H. Li, T. Li, A. Luo, W. Xu, Z. Luo, *Laser Photonics Rev.* **2020**, *14*, 1900317.

[135] Z. Wang, A. Coillet, S. Hamdi, Z. Zhang, P. Grelu, *Laser Photonics Rev.* **2023**, *17*, 2200298.

[136] Y. Du, X. Shu, *Opt. Express* **2018**, *26*, 5564.

[137] A. F. J. Runge, N. G. R. Broderick, M. Erkintalo, *Optica* **2014**, *2*, 36.

[138] J. Peng, H. Zeng, *Commun. Phys.* **2019**, *2*, 1.

[139] Z. W. Wei, M. Liu, S. X. Ming, H. Cui, A. P. Luo, W. C. Xu, Z. C. Luo, *Opt. Lett.* **2020**, *45*, 531.

[140] Y. Yu, Z.-C. Luo, J. Kang, K. K. Y. Wong, *Opt. Lett.* **2018**, *43*, 4132.

[141] K. Krupa, K. Nithyanandan, P. Grelu, *Optica* **2017**, *4*, 1239.

[142] S. T. Cundiff, J. M. Soto-Crespo, N. Akhmediev, *Phys. Rev. Lett.* **2002**, *88*, 073903.

[143] J. Zeng, M. Y. Sander, *Opt. Express* **2022**, *30*, 7894.

[144] D. Rand, I. Glesk, C. Brès, D. A. Nolan, X. Chen, J. Koh, J. W. Fleischer, K. Steiglitz, P. R. Prucnal, *Phys. Rev. Lett.* **2007**, *98*, 053902.

[145] Y. Cui, Y. Zhang, Y. Song, L. Huang, L. Tong, J. Qiu, X. Liu, *Laser Photonics Rev.* **2021**, *15*, 2000216.

[146] M. Liu, A.-P. Luo, Z.-C. Luo, W.-C. Xu, *Opt. Lett.* **2017**, *42*, 330.

[147] V. V. Afanasjev, *Opt. Lett.* **1995**, *20*, 270.

[148] D. R. Solli, C. Ropers, P. Koonath, B. Jalali, *Nature* **2007**, *450*, 1054.

[149] A. Zaviyalov, O. Egorov, R. Iliew, F. Lederer, *Phys. Rev. A* **2012**, *85*, 013828.

[150] J. M. Soto-Crespo, P. Grelu, N. Akhmediev, *Phys. Rev. E* **2011**, *84*, 016604.

[151] C. Lecaplain, P. Grelu, *Phys. Rev. A* **2014**, *90*, 013805.

[152] Z. Liu, S. Zhang, F. W. Wise, *Opt. Lett.* **2015**, *40*, 1366.

[153] M. Liu, A.-P. Luo, W.-C. Xu, Z.-C. Luo, *Opt. Lett.* **2016**, *41*, 3912.

[154] M. Luo, Z. X. Zhang, M. Liu, A. P. Luo, W. C. Xu, Z. C. Luo, *Opt. Express* **2022**, *30*, 22143.

[155] Z. R. Cai, M. Liu, S. Hu, J. Yao, A. P. Luo, Z. C. Luo, W. C. Xu, *IEEE J. Sel. Top. Quantum Electron.* **2017**, *23*, 20.

[156] A. F. J. Runge, C. Aguergaray, N. G. R. Broderick, M. Erkintalo, *Opt. Lett.* **2014**, *39*, 319.

[157] A. F. J. Runge, C. Aguergaray, N. G. R. Broderick, M. Erkintalo, *Opt. Lett.* **2013**, *38*, 4327.

[158] W. H. Renninger, A. Chong, F. W. Wise, *Phys. Rev. A* **2008**, *77*, 023814.

[159] Z. C. Luo, J. Q. Kang, M. Liu, C. Li, C. H. Kong, Y. Yu, K. K. Wong, *IEEE Photonics Technol. Lett.* **2018**, *30*, 1803.

[160] R.-Q. Xu, Y.-R. Song, Z.-K. Dong, K. Li, J. Tian, *Appl. Opt.* **2017**, *56*, 1674.

[161] Z. Wang, C. Ma, Y. Song, J. Liu, H. Zhu, Y. Duan, H. Zhang, *Opt. Express* **2020**, *28*, 39463.

[162] Z. Wang, K. Nithyanandan, A. Coillet, P. Tchofo-Dinda, P. Grelu, *Phys. Rev. Res.* **2020**, *2*, 013101.

[163] A. Martinez, Z. Sun, *Nat. Photonics* **2013**, *7*, 842.

[164] X. Bao, H. Mu, Y. Chen, P. Li, L. Li, S. Li, K. Qasim, Y. Zhang, H. Zhang, Q. Bao, *J. Phys. D: Appl. Phys.* **2018**, *51*, 375106.

[165] Y. I. Jhon, J. Koo, B. Anasori, M. Seo, J. H. Lee, Y. Gogotsi, Y. M. Jhon, *Adv. Mater.* **2017**, *29*, 1702496.

[166] K. Zhao, C. Gao, X. Xiao, C. Yang, *Opt. Lett.* **2020**, *45*, 4040.

[167] S. Xu, A. Turnali, M. Y. Sander, *Sci. Rep.* **2022**, *12*, 6841.

[168] S. Kivisto, J. Puustinen, M. Guina, O. G. Okhotnikov, E. M. Dianov, *Electron. Lett.* **2005**, *44*, 1456.

[169] E. M. Dianov, *Light: Sci. Appl.* **2012**, *1*, e12.

[170] R. Gumenyuk, J. Puustinen, A. V. Shubin, I. A. Bufetov, E. M. Dianov, O. G. Okhotnikov, *Opt. Lett.* **2013**, *38*, 4005.

[171] T. Noronen, M. Melkumov, D. Stolyarov, V. F. Khopin, E. Dianov, O. G. Okhotnikov, *Opt. Lett.* **2015**, *40*, 2217.

[172] A. Khegai, M. Melkumov, S. Firstov, K. Riumkin, Y. Gladush, S. Alyshev, A. Lobanov, V. Khopin, F. Afanasiev, A. G. Nasibulin, E. Dianov, *Opt. Express* **2018**, *26*, 23911.

[173] J. Huang, M. Pang, X. Jiang, W. He, P. S. Russell, *Opt. Express* **2019**, *27*, 26392.

[174] J. Zou, C. Dong, H. Wang, T. Du, Z. Luo, *Light: Sci. Appl.* **2020**, *9*, 61.

[175] Q. Ruan, X. Xiao, J. Zou, H. Wang, S. Fan, T. Li, J. Li, Z. Dong, Z. Cai, Z. Luo, *Laser Photonics Rev.* **2022**, *16*, 2100678.

[176] H. Sun, L. Wang, J. Zou, Q. Ruan, Y. Ding, C. Dong, Z. Dong, Z. Luo, *J. Light. Technol.* **2022**, *40*, 191.

[177] J. Zou, J. Hong, Z. Zhao, Q. Li, Q. Ruan, H. Wang, Y. Bu, X. Guan, M. Zhou, Z. Feng, Z. Luo, *Adv. Photonics* **2022**, *4*, 056001.

[178] B. H. Kolner, *IEEE J. Quantum Electron.* **1994**, *30*, 1951.

[179] Y. Zhang, L. Huang, Y. Cui, X. Liu, *Opt. Lett.* **2020**, *45*, 4835.

[180] P. Suret, R. E. Koussaifi, A. Tikan, C. Evain, S. Randoux, C. Szwaj, S. Bielawski, *Nat. Commun.* **2016**, *7*, 13136.

[181] M. Närhi, B. Wetzel, C. Billet, S. Toenger, T. Sylvestre, J. M. Merolla, R. Morandotti, F. Dias, G. Genty, J. M. Dudley, *Nat. Commun.* **2016**, *7*, 13675.

[182] Y. Zhang, Y. Cui, L. Huang, L. Tong, X. Liu, *Opt. Lett.* **2020**, *45*, 6246.
[183] Y. Zhang, S. Luo, B. Zhang, Y. Cui, Q. Ling, Z. Yu, D. Chen, *Opt. Laser Technol.* **2022**, *153*, 108286.
[184] B. Li, J. Kang, S. Wang, Y. Yu, P. Feng, K. K. Y. Wong, *Opt. Lett.* **2019**, *44*, 4351.

[185] A. Klein, G. Masri, H. Duadi, K. Sulimany, O. Lib, H. Steinberg, S. A. Kolpakov, M. Fridman, *Optica* **2018**, *5*, 774.
[186] X. Wu, J. Peng, S. Boscolo, Y. Zhang, C. Finot, H. Zeng, *Laser Photonics Rev.* **2022**, *16*, 2100191.
[187] W. H. Renninger, F. W. Wise, *Optica* **2014**, *1*, 101.

Kuen Yao Lau received his Ph.D. degree in Photonics Engineering from Universiti Putra Malaysia in 2018. After his graduation, he joined Universiti Tenaga Nasional, Malaysia, and Aalto University, Finland, as a postdoctoral researcher from 2018–2019 and 2019–2020, respectively. Currently, he is appointed as a National-Funded postdoctoral researcher in Zhejiang University, China. His research interests include fiber lasers, saturable absorbers, modulators, mode-locking, and ultrafast optics.

Yudong Cui received his Ph.D. in Optical Engineering from the University of Chinese Academy of Sciences. From 2016 to 2018, he was engaged in postdoctoral research at Zhejiang University and currently works in the College of Optical Science and Engineering at Zhejiang University. His research interests include nonlinear optics of nanomaterials, high-energy ultrafast fiber lasers, time-stretched dispersive Fourier transformation, time lens, and related applications.

Xiaofeng Liu received his Ph.D. degree in Materials Science from the Shanghai Institute of Optics and Fine Mechanics, Chinese Academy of Science, China, in 2011. Later, he joined the Frontier Research Center, Tokyo Institute of Technology, Japan, and the Max Planck Institute of Colloids and Interfaces, Germany, as a Humboldt postdoctoral fellow. Currently, he is an associate professor in the School of Materials Science and Engineering, Zhejiang University, China. His research interests include optical properties of materials and nonlinear optical properties and devices.

Jianrong Qiu received his Ph.D. degree from Okayama University, Japan, in 1992. Later, he joined the New Glass Research Center of Yamamura Glass Co. Ltd., Japan, from 1992 to 1994, and worked as chief researcher in the Hirao Active Glass Project, Japan, from 1995 to 1999 and as group leader of the Photon Craft International Cooperative Research Project in Kyoto University, Japan, from 2000 to 2004. Currently, he is a professor in the College of Optical Science and Engineering, Zhejiang University, China. His research interests include femtosecond laser interaction with matter and applications, luminescent materials, and nonlinear optical materials and devices.

2200763 (32 of 32)